A wavelet based sparse grid method for the electronic Schrödinger equation

Michael Griebel and Jan Hamaekers*

Abstract. We present a direct discretization of the electronic Schrödinger equation. It is based on one-dimensional Meyer wavelets from which we build an anisotropic multiresolution analysis for general particle spaces by a tensor product construction. We restrict these spaces to the case of antisymmetric functions. To obtain finite-dimensional subspaces we first discuss semi-discretization with respect to the scale parameter by means of sparse grids which relies on mixed regularity and decay properties of the electronic wave functions. We then propose different techniques for a discretization with respect to the position parameter. Furthermore we present the results of our numerical experiments using this new generalized sparse grid methods for Schrödinger's equation.

Mathematics Subject Classification (2000). 35J10, 65N25, 65N30, 65T40, 65Z05.

Keywords. Schrödinger equation, numerical approximation, sparse grid method, antisymmetric sparse grids.

1. Introduction

In this article we consider the electronic Schrödinger equation (first without spin for reasons of simplicity)

$$H\Psi(\boldsymbol{x}_1,\ldots,\boldsymbol{x}_N) = E\Psi(\boldsymbol{x}_1,\ldots,\boldsymbol{x}_N) \tag{1}$$

with the Hamilton operator

$$H = T + V \quad \text{where } T = -\frac{1}{2}\sum_{p=1}^{N}\Delta_p$$

and

$$V = -\sum_{p=1}^{N}\sum_{q=1}^{N_{\text{nuc}}}\frac{Z_q}{|\boldsymbol{x}_p - \boldsymbol{R}_q|_2} + \sum_{p=1}^{N}\sum_{q>p}^{N}\frac{1}{|\boldsymbol{x}_p - \boldsymbol{x}_q|_2}. \tag{2}$$

*The authors were supported in part by the priority program 1145 *Modern and universal first-principles methods for many-electron systems in chemistry and physics* and the Sonderforschungsbereich 611 *Singuläre Phänomene und Skalierung in Mathematischen Modellen* of the Deutsche Forschungsgemeinschaft.

Proceedings of the International Congress
of Mathematicians, Madrid, Spain, 2006

Here, with $d = 3$, $\boldsymbol{x}_p := (x_{1,p}, \ldots, x_{d,p}) \in \mathbb{R}^d$ denotes the position of the p-th electron, $p = 1 \ldots, N$, and $\boldsymbol{R}_q \in \mathbb{R}^d$ denotes the fixed position of the q-th nucleus, $q = 1, \ldots, N_{\text{nuc}}$. The operator Δ_p is the Laplacian acting on the $\boldsymbol{x}_p$-component of Ψ, i.e. $\Delta_p = \sum_{i=1}^{d} \partial^2/\partial(x_{i,p})^2$, Z_q is the charge of the q-th nucleus and the norm $|\,.\,|_2$ denotes the usual Euclidean distance in $\mathbb{R}^d$. The solution Ψ describes the wave function associated to the eigenvalue E.

This eigenvalue problem results from the Born–Oppenheimer approximation [51] to the general Schrödinger equation for a system of electrons and nuclei which takes the different masses of electrons and nuclei into account. It is one of the core problems of computational chemistry. Its successful treatment would allow to predict the properties of arbitrary atomic systems and molecules [22]. However, except for very simple cases, there is no analytical solution for (1) available. Also a direct numerical approach is impossible since Ψ is a $d \cdot N$-dimensional function. Any discretization on e.g. uniform grids with $O(K)$ points in each direction would involve $O(K^{d \cdot N})$ degrees of freedoms which are impossible to store for $d = 3$, $N > 1$. Here, we encounter the curse of dimensionality [8]. Therefore, most approaches resort to an approximation of (1) only. Examples are the classical Hartree–Fock method and its successive refinements like configuration interaction and coupled clusters. Alternative methods are based on density functional theory which result in the Kohn–Sham equations or the reduced density matrix (RDM) [50] and the r12 approach [23] which lead to improved accuracy and open the way to new applications. A survey of these methods can be found in [3], [10], [46]. A major problem with these techniques is that, albeit quite successful in practice, they nevertheless only provide approximations. A systematical improvement is usually not available such that convergence of the model to Schrödinger's equation is achieved.

Instead, we intend to directly discretize the Schrödinger equation without resorting to any model approximation. To this end, we propose a new variant of the so-called sparse grid approach. The sparse grid method is a discretization technique for higher-dimensional problems which promises to circumvent the above-mentioned curse of dimensionality provided that certain smoothness prerequisites are fulfilled. Various sparse grid discretization methods have already been developed in the context of integration problems [27], [28], integral equations [24], [32] and elliptic partial differential equations, see [12] and the references cited therein for an overview. In Fourier space, such methods are also known under the name hyperbolic cross approximation [5], [21], [61]. A first heuristic approach to apply this methodology to the electronic Schrödinger equation was presented in [26]. The sparse grid idea was also used in the fast evaluation of Slater determinants in [33]. Recently Yserentant showed in [67] that the smoothness prerequisite necessary for sparse grids is indeed valid for the solution of the electronic Schrödinger equation. To be more precise, he showed that an antisymmetric solution of the electronic Schrödinger equation with $d = 3$ possesses $\mathcal{H}^{1,1}_{\text{mix}}$- or $\mathcal{H}^{1/2,1}_{\text{mix}}$-regularity for the fully antisymmetric and the partially symmetric case, respectively. This motivated the application of a generalized sparse grid approach in Fourier space to the electronic Schrödinger equation as presented

in [30]. There, sparse grids for general particle problems as well as antisymmetric sparse grids have been developed and were applied to (1) in the periodic setting. Basically, estimates of the type

$$\|\Psi - \Psi_M\|_{\mathcal{H}^1} \leq C(N,d) \cdot M^{-1/d} \cdot \|\Psi\|_{\mathcal{H}^{1,1}_{\text{mix}}}$$

could be achieved where M denotes the number of Fourier modes used in the discretization. Here, the norm $\|.\|_{\mathcal{H}^{1,1}_{\text{mix}}}$ involves bounded mixed first derivatives. Thus the order of the method with respect to M is asymptotically independent of the dimension of the problem, i.e. the number N of electrons. But, the constants and the $\mathcal{H}^{1,1}_{\text{mix}}$-norm of the solution nevertheless depend on the number of electrons. While the dependency of the order constant might be analysed along the lines of [29], the problem remains that the smoothness term $\|\Psi\|_{\mathcal{H}^{1,1}_{\text{mix}}}$ grows exponentially with the number of electrons. This could be seen from the results of the numerical experiments in [30] and was one reason why in the periodic Fourier setting problems with higher numbers of electrons could not be treated. It was also observed in [69] where a certain scaling was introduced into the definitions of the norms which compensates for this growth factor. In [68], [70] it was suggested to scale the decomposition of the hyperbolic cross into subspaces accordingly and to further approximate each of the subspace contributions by some individually properly truncated Fourier series to cope with this problem.

In this article, we present a modified sparse grid/hyperbolic cross discretization for the electronic Schrödinger equation which implements this approach. It uses one-dimensional Meyer wavelets as basic building blocks in a tensor product construction to obtain a $\mathcal{L}^2$-orthogonal multiscale basis for the many-electron space. Then a truncation of the associated series expansion results in sparse grids. Here, for the level index we truncate according to the idea of hyperbolic crosses whereas we truncate for the position index according to various patterns which take to some extent the decay of the scaling function coefficients for $x \to \infty$ into account. Note that since we work in an infinite domain this resembles a truncation to a compact domain in which we then consider a local wavelet basis. Here, domain truncation error and scale resolution error should be balanced. Antisymmetry of the resulting discrete wavelet basis is achieved by a restriction of the active indices.

The remainder of this article is organized as follows: In Section 2 we present the Meyer wavelet family on $\mathbb{R}$ and discuss its properties. In Section 3 we introduce a multiresolution analysis for many particle spaces build by a tensor product construction from the one-dimensional Meyer wavelets and introduce various Sobolev norms. Then we discuss semi-discretization with respect to the scale parameter by means of generalized sparse grids and present a resulting error estimate in Section 4. Section 5 deals with antisymmetric generalized sparse grids. In Section 6 we invoke results on the mixed regularity of electronic wave functions and we discuss rescaling of norms and sparse grid spaces to obtain error bounds which involve the $\mathcal{L}^2$-norm of the solution instead of the mixed Sobolev norm. Then, in Section 7 we comment on the setup

of the system matrix and on the solution procedure for the discrete eigenvalue problem on general sparse grids and we propose different techniques for the discretization with respect to the position parameter. Furthermore we present the results of our numerical experiments. Finally we give some concluding remarks in Section 8.

2. Orthogonal multilevel bases and the Meyer wavelet family on $\mathbb{R}$

We intend to use for the discretization of (1) a $\mathcal{L}^2$-orthogonal basis system.[1] This is an important prerequisite from the practical point of view, since it allows to apply the well-known Slater–Condon rules. They reduce the $\mathbb{R}^{d\cdot N}$- and $\mathbb{R}^{2\cdot d\cdot N}$-dimensional integrals necessary in the Galerkin discretization of the one- and two electron part of the potential function of (1) to short sums of d-dimensional and $2d$-dimensional integrals, respectively. Otherwise, due to the structure of the Slater determinants necessary to obtain antisymmetry, these sums would contain exponentially many terms with respect to the number N of electrons present in the system.

Let us recall the definition of a multiresolution analysis on $\mathbb{R}$, see also [52]. We consider an infinite sequence

$$\cdots \subset V_{-2} \subset V_{-1} \subset V_0 \subset V_1 \subset V_2 \subset \cdots$$

of nested spaces V_l with $\bigcap_{l\in\mathbb{Z}} V_l = 0$ and $\overline{\bigcup_{l\in\mathbb{Z}} V_l} = \mathcal{L}^2(\mathbb{R})$. It holds $f(x) \in V_l \Leftrightarrow f(2x) \in V_{l+1}$ and $f(x) \in V_0 \Leftrightarrow f(x-j) \in V_0$, where $j \in \mathbb{Z}$. Furthermore, there is a so-called scaling function (or father wavelet) $\phi \in V_0$, such that $\{\phi(x-j) \,:\, j \in \mathbb{Z}\}$ forms an orthonormal basis for V_0. Then

$$\{\phi_{l,j}(x) = 2^{\frac{l}{2}}\phi(2^l x - j) \,:\, j \in \mathbb{Z}\}$$

forms an orthonormal basis of V_l and we can represent any $u(x) \in V_l$ as $u(x) = \sum_{j=-\infty}^{\infty} v_{l,j}\phi_{l,j}(x)$ with coefficients $v_{l,j} := \int_{\mathbb{R}} \phi^*_{l,j}(x)u(x)dx$. With the definition

$$W_l \perp V_l,\ V_l \oplus W_l = V_{l+1} \tag{3}$$

we obtain an associated sequence of detail spaces W_l with associated mother wavelet $\varphi \in W_0$, such that $\{\varphi(x-j) \,:\, j \in \mathbb{Z}\}$ forms an orthonormal basis for W_0. Thus

$$\{\varphi_{l,j}(x) = 2^{\frac{l}{2}}\varphi(2^l x - j) \,:\, j \in \mathbb{Z}\}$$

gives an orthonormal basis for W_l and $\{\varphi_{l,j} \,:\, l, j \in \mathbb{Z}\}$ is an orthonormal basis of $\mathcal{L}^2(\mathbb{R})$. Then, we can represent any $u(x)$ in $\mathcal{L}^2(\mathbb{R})$ as

$$u(x) = \sum_{l=-\infty}^{\infty} \sum_{j=-\infty}^{\infty} u_{l,j}\varphi_{l,j}(x) \tag{4}$$

[1] Note that a bi-orthogonal system would also work here.

with the coefficients $u_{l,j} := \int_{\mathbb{R}} \varphi^*_{l,j}(x)u(x)dx$.

In the following we focus on the Meyer wavelet family for the choice of ϕ and φ. There, with the definition of the Fourier transform $\mathcal{F}[f](\omega) = \hat{f}(\omega) = \frac{1}{\sqrt{2\pi}} \int_{-\infty}^{\infty} f(x)e^{-i\omega x}\,dx$ we set as father and mother wavelet in Fourier space

$$\hat{\phi}(\omega) = \frac{1}{\sqrt{2\pi}} \begin{cases} 1 & \text{for } |\omega| \leq \frac{2}{3}\pi, \\ \cos(\frac{\pi}{2}\nu(\frac{3}{2\pi}|\omega| - 1)) & \text{for } \frac{2\pi}{3} < |\omega| \leq \frac{4\pi}{3}, \\ 0 & \text{otherwise,} \end{cases} \tag{5}$$

$$\hat{\varphi}(\omega) = \frac{1}{\sqrt{2\pi}} e^{-i\frac{\omega}{2}} \begin{cases} \sin(\frac{\pi}{2}\nu(\frac{3}{2\pi}|\omega| - 1)) & \text{for } \frac{2}{3}\pi \leq |\omega| \leq \frac{4}{3}\pi, \\ \cos(\frac{\pi}{2}\nu(\frac{3}{4\pi}|\omega| - 1)) & \text{for } \frac{4\pi}{3} < |\omega| \leq \frac{8\pi}{3}, \\ 0 & \text{otherwise,} \end{cases} \tag{6}$$

where $\nu\colon \mathbb{R} \to \mathbb{R} \in C^r$ is a parameter function still do be fixed, which has the properties $\nu(x) = 0$ for $x \leq 0$, $\nu(x) = 1$ for $x > 1$ and $\nu(x) + \nu(1 - x) = 1$. By dilation and translation we obtain

$$\mathcal{F}[\phi_{l,j}](\omega) = \hat{\phi}_{l,j}(\omega) = 2^{-\frac{l}{2}} e^{-i2^{-l}j\omega} \hat{\phi}(2^{-l}\omega),$$
$$\mathcal{F}[\varphi_{l,j}](\omega) = \hat{\varphi}_{l,j}(\omega) = 2^{-\frac{l}{2}} e^{-i2^{-l}j\omega} \hat{\varphi}(2^{-l}\omega)$$

where the $\hat{\phi}_{l,j}$ and $\hat{\varphi}_{l,j}$ denote the dilates and translates of (5) and (6), respectively.

This wavelet family can be derived from a partition of unity $\sum_l \hat{\chi}_l(\omega) = 1$ for all $\omega \in \mathbb{R}$ in Fourier space, where

$$\hat{\chi}_l(\omega) = \begin{cases} 2\pi \hat{\phi}^*_{0,0}(\omega)\hat{\phi}_{0,0}(\omega) & \text{for } l = 0, \\ 2^l \pi \hat{\varphi}^*_{l-1,0}(\omega)\hat{\varphi}_{l-1,0}(\omega) & \text{for } l > 0, \end{cases} \tag{7}$$

see [4] for details. The function ν basically describes the decay from one to zero of one partition function $\hat{\chi}_l$ in the overlap with its neighbor. The smoothness of the $\hat{\chi}_l$ is thus directly determined by the smoothness of ν. The mother wavelets $\hat{\varphi}_{l,j}$ and the father wavelets $\hat{\phi}_{l,j}$ in Fourier space inherit the smoothness of the $\hat{\chi}_l$'s via the relation (7).

There are various choices for ν with different smoothness properties in the literature, see [4], [45], [53], [54]. Examples are the Shannon wavelet and the raised cosine wavelet [63], i.e. (6) with

$$\nu(x) = \nu^0(x) := \begin{cases} 0 & \text{for } x \leq \frac{1}{2}, \\ 1 & \text{otherwise} \end{cases} \quad \text{and} \quad \nu(x) = \nu^1(x) \begin{cases} 0 & \text{for } x \leq 0, \\ x & \text{for } 0 \leq x \leq 1, \\ 1 & \text{otherwise} \end{cases} \tag{8}$$

or, on the other hand,

$$\nu(x) = \nu^{\infty}(x) := \begin{cases} 0 & \text{for } x \leq 0 \\ \frac{\tilde{\nu}(x)}{\tilde{\nu}(1-x)+\tilde{\nu}(x)} & \text{for } 0 < x \leq 1 \\ 1 & \text{otherwise} \end{cases} \quad \text{where } \tilde{\nu}(x) = \begin{cases} 0 & \text{for } x \leq 0 \\ e^{-\frac{1}{x^{\alpha}}} & \text{otherwise} \end{cases} \tag{9}$$

with $\alpha = 1, 2$ [62], respectively. Other types of Meyer wavelets with different smoothness properties can be found in [19], [34], [40], [65]. The resulting mother wavelet functions in real space and Fourier space are given in Figure 1. Note the

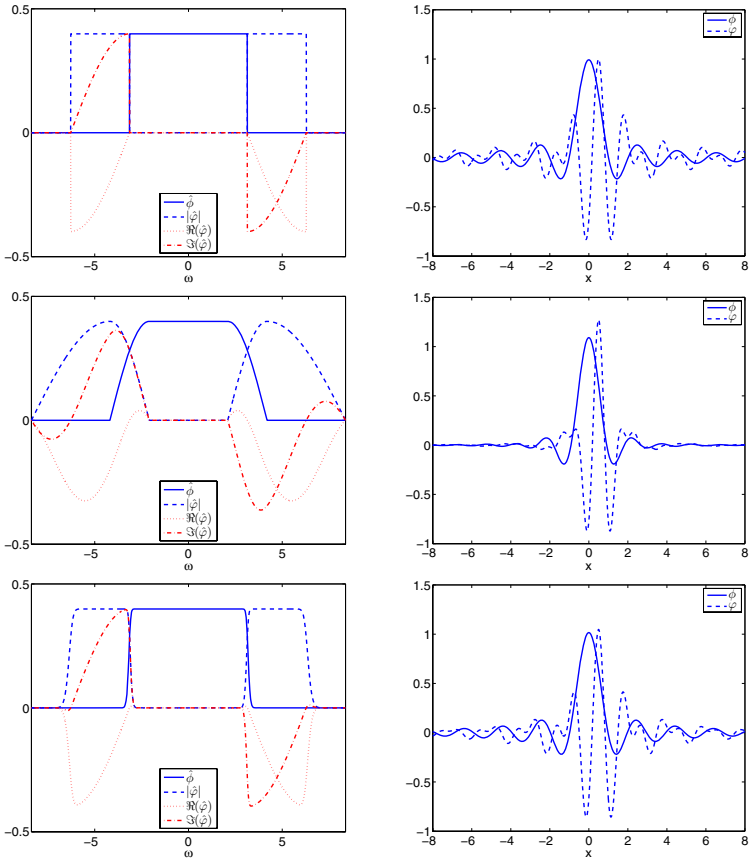

Figure 1. Top: (6) with ν^0 from (8) in Fourier space (left) and real space (right). Middle: (6) with ν^1 from (8) in Fourier space (left) and real space (right). Bottom: (6) with ν^{∞} from (9) in Fourier space (left) and real space (right).

two symmetric areas of support and the associated two bands with non-zero values of the wavelets in Fourier space which resemble the line of construction due to Wilson,

Malvar, Coifman and Meyer [17], [20], [39], [49], [64] to circumvent the Balian–Low theorem[2] [7], [48]. In real space, these wavelets are C^∞-functions with global support, in Fourier space, they are piecewise continuous, piecewise continuous differentiable and C^∞, respectively, and have compact support. Furthermore they possess infinitely many vanishing moments. Finally their envelope in real space decays with $|x| \to \infty$ as $|x|^{-1}$ for ν^0, as $|x|^{-2}$ for ν^1 and faster than any polynomial (subexponentially) for ν^∞, respectively. To our knowledge, only for the Meyer wavelets with (8) there are analytical formulae in both real and Fourier space available. Certain integrals in a Galerkin discretization of (1) can then be given analytically. For the other types of Meyer wavelets analytical formulae only exist in Fourier space and thus numerical integration is necessary in a Galerkin discretization of (1).

For a discretization of (4) with respect to the level-scale l we can restrict the doubly infinite sum to an interval, i.e. $l \in [L_1, L_2]$. However to obtain the space V_{L_2} we have to complement the sum of detail spaces W_l, $l \in [L_1, L_2]$ by the space V_{L_1}, i.e. we have

$$V_{L_2} = V_{L_1} \oplus \bigoplus_{l=L_1}^{L_2} W_l.$$

with the associated representation

$$u(x) = \sum_{j=-\infty}^{\infty} v_{L_1,j}\phi_{L_1,j}(x) + \sum_{L_1}^{L_2}\sum_{j=-\infty}^{\infty} u_{l,j}\varphi_{l,j}(x).$$

Note that for the case of $\mathbb{R}$, beside the choice of a finest scale L_2, we here also have a choice of the coarsest scale L_1. This is in contrast to the case of a finite domain where the coarsest scale is usually determined by the size of the domain and is denoted as level zero.

Additionally we can scale our spaces and decompositions by a parameter $c > 0$, $c \in \mathbb{R}$. For example, we can set

$$V_l^c = \operatorname{span}\{\phi_{c,l,j}(x) = c^{\frac{1}{2}} 2^{\frac{l}{2}} \phi(c2^l x - j) \ : \ j \in \mathbb{Z}\}.$$

For $c = 2^k$, $k \in \mathbb{Z}$, the obvious identity $V_l^c = V_{l+k}^1$ holds. Then we obtain the scaled decomposition

$$V_{L_2}^c = V_{L_1}^c \oplus \bigoplus_{l=L_1}^{L_2} W_l^c$$

with the scaled detail spaces $W_l^c = \operatorname{span}\{\varphi_{c,l,j}(x) = c^{\frac{1}{2}} 2^{\frac{l}{2}} \varphi(c2^l x - j) \ : \ j \in \mathbb{Z}\}$. For $c = 2^k$, $k \in \mathbb{Z}$, the identity $W_l^c = W_{l+k}^1$ holds.

[2]The Balian–Low theorem basically states that the family of functions $g_{m,n}(x) = e^{2\pi i m x} g(x-n), m, n \in \mathbb{Z}$, which are related to the windowed Fourier transform, cannot be an orthonormal basis of $\mathcal{L}^2(\mathbb{R})$, if the two integrals $\int_{\mathbb{R}} x^2 |g(x)|^2 dx$ and $\int_{\mathbb{R}} k^2 |\hat{g}(k)|^2 dk$ are both finite. Thus there exists no orthonormal family for a Gaussian window function $g(x) = \pi^{-1/4} e^{-x^2/2}$ which is both sufficiently regular and well localized.

With the choice $c = 2^{-L_1}$ we can get rid of the parameter L_1 and may write our wavelet decomposition as

$$V_L^c = V_0^c \oplus \bigoplus_{l=0}^{L} W_l^c, \tag{10}$$

i.e. we can denote the associated coarsest space with level zero and the finest detail space with level L (which now expresses the rescaled parameter L_2). To simplify notation we will skip the scaling index c in the following.

We also introduce with

$$\psi_{l,j} := \begin{cases} \phi_{l,j}^c & \text{for } l = 0, \\ \varphi_{l-1,j}^c & \text{for } l \geq 1 \end{cases} \tag{11}$$

for $c = 2^{-L_1}$ a unique notation for both the father wavelets on the coarsest scale and the mother wavelets of the detail spaces. Bear however in mind that in the following the function $\psi_{l,j}$ with $l = 0$ denotes a father wavelet, i.e. a scaling function only, whereas it denotes for $l \geq 1$ a true wavelet on scale $l - 1$.

Let us finally consider the wavelet representation of the function $e^{-\sigma|x-x_0|}$ which is the one-dimensional analogon of the ground state wavefunction of hydrogen centered in $x_0 = 0$. For two types of Meyer wavelets, i.e. with ν^0 from (8) and ν^∞ from (9) with $\alpha = 2$, Figure 2 gives the isolines to the values 10^{-3} and 10^{-4} for both the absolute value of the coefficients $v_{l,j}$ of the representation with respect to the scaling functions and the absolute value of the coefficients $u_{l,j}$ of the representation with respect to the wavelet functions.

Here we see the following: For the Meyer wavelet with ν^∞ from (9) where $\alpha = 2$, the isolines to different values (only 10^{-3} and 10^{-4} are shown) are nearly parallel for both the wavelet coefficients $u_{l,j}$ and the scaling coefficients $v_{l,j}$. For levels larger than -2 the isolines of the wavelet coefficients are even straight lines. Furthermore, on sufficiently coarse levels, the isoline for the wavelet coefficients and the scaling coefficients practically coincide. This is an effect of the C^∞-property of the underlying mother wavelet. For the Meyer wavelet with ν^0 from (8), i.e. for wavelets which are not C^∞ in both real space *and* Fourier space, these two observations do not hold.

If we compare the isolines of the wavelet coefficients $u_{l,j}$ for the Meyer wavelet with ν^∞ from (9) where $\alpha = 2$ and that of the Meyer wavelet with ν^0 from (8) we observe that the level on which the bottom kink occurs is exactly the same. However the size of the largest diameter (here roughly on level -2) is substantially bigger for the Shannon wavelet. Note the different scaling of the x-axis of the diagrams on the left and right side.

We furthermore observe for the isolines of the scaling coefficients an exponential behavior, i.e. from level l to level $l + 1$ the associated value for j nearly doubles in a sufficient distance away from point $x = 0$. With respect to the wavelet coefficients, however, we see that the support shrinks super-exponentially towards the bottom kink with raising level.

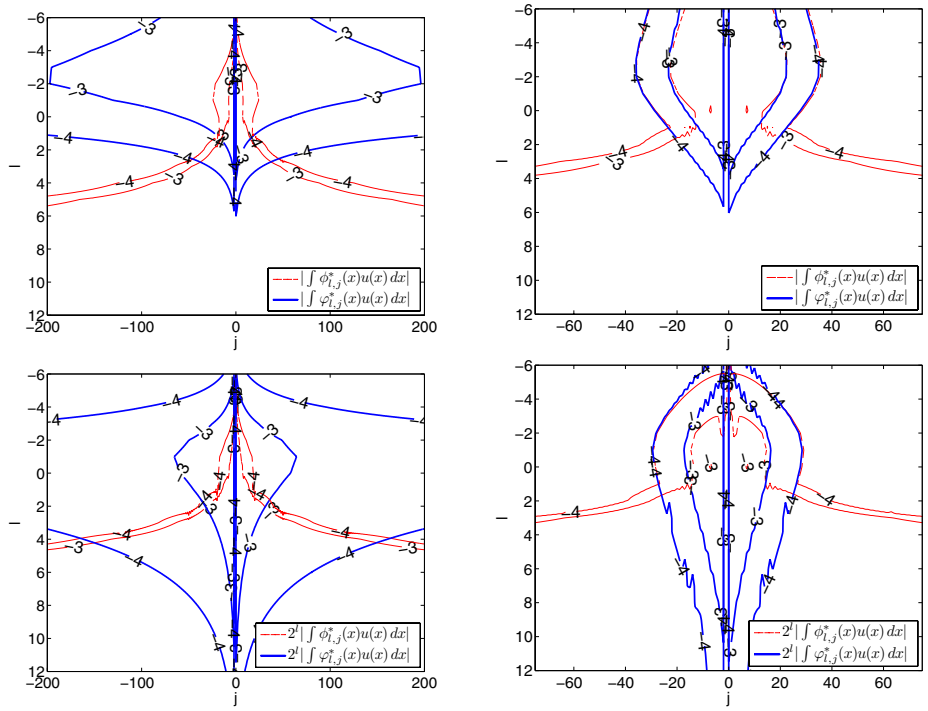

Figure 2. Isolines to the values 10^{-3} and 10^{-4} of the absolute value of the coefficients $v_{l,j}$ and $u_{l,j}$ for the Meyer wavelets with ν^0 from (8) (left) and ν^∞ from (9) with $\alpha = 2$ (right), no scaling (top) and scaling with 2^l (bottom).

The relation (3) relates the spaces V_l, W_l and V_{l+1} and allows to switch between the scaling coefficients and the wavelet coefficients on level l to the scaling coefficients on level $l+1$ and vice versa. This enables us to choose an optimal coarsest level for a prescribed accuracy and we also can read off the pattern of indices (l, j) which result in a best M-term approximation with respect to the $\mathcal{L}^2$- and $\mathcal{H}^1$-norm for that prescribed accuracy, respectively. For the Meyer wavelet with ν^∞ from (9) where $\alpha = 2$, the optimal choice of the coarsest level L_1 on which we use scaling functions is just the level where, for a prescribed accuracy, the two absolute values of the wavelet coefficients on one level possess their largest distance, i.e. the associated isoline of the wavelet coefficients shows the largest diameter (here roughly on level -2). The selection of a crossing isoline then corresponds to the fixation of a boundary error by truncation of the further decaying scaling function coefficients on that level which resembles a restriction of $\mathbb{R}$ to just a finite domain. From this base a downward pointing triangle then gives the area of indices to be taken into account into the finite sum of best approximation with respect to that error. We observe that the use of the wavelets with ν^0 from (8) would result in a substantially larger area of indices and

thus number of coefficients to be taken into account to obtain the same error level. There, the form of the area is no longer a simple triangle but shows a "butterfly"-like shape where the base of the pattern is substantially larger.

3. MRA and Sobolev spaces for particle spaces

In the following we introduce a multiresolution analysis based on Meyer wavelets for particle spaces on $(\mathbb{R}^d)^N$ and discuss various Sobolev spaces on it.

First, let us set up a basis for the one-particle space $\mathcal{H}^s(\mathbb{R}^d) \subset \mathcal{L}^2(\mathbb{R}^d)$. Here, we use the d-dimensional product of the one-dimensional system $\{\psi_{l,j}(x), l \in \mathbb{N}_0, j \in \mathbb{Z}\}$. We then define the d-dimensional multi-indices $\boldsymbol{l} = (l_1, l_2, \ldots, l_d) \in \mathbb{N}_0^d$ and $\boldsymbol{j} = (j_1, j_2, \ldots, j_d) \in \mathbb{Z}^d$, the coordinate vector $\boldsymbol{x} = (x_1, \ldots, x_d) \in \mathbb{R}^d$ and the associated d-dimensional basis functions

$$\psi_{\boldsymbol{l},\boldsymbol{j}}(\boldsymbol{x}) := \prod_{i=1}^{d} \psi_{l_i,j_i}(x_i). \tag{12}$$

Note that due to (11) this product may involve both father and mother wavelets depending on the values of the components of the level index $\boldsymbol{l}$. We furthermore denote $|\boldsymbol{l}|_2 = \left(\sum_{i=1}^d l_i^2\right)^{1/2}$ and $|\boldsymbol{l}|_\infty = \max_{1\le i\le d} |l_i|$. Let us now define isotropic Sobolev spaces in d dimensions with help of the wavelet series expansion, i.e. we classify functions via the decay of their wavelet coefficients. To this end, we set

$$\lambda(\boldsymbol{l}) := |2^{\boldsymbol{l}}|_2 = |(2^{l_1}, \ldots, 2^{l_d})|_2 \tag{13}$$

and define

$$\begin{aligned}\mathcal{H}^s(\mathbb{R}^d) = \Big\{u(\boldsymbol{x}) = \sum\nolimits_{\substack{l\in\mathbb{N}_0^d,\\ \boldsymbol{j}\in\mathbb{Z}^d}} u_{\boldsymbol{l},\boldsymbol{j}}\psi_{\boldsymbol{l},\boldsymbol{i}}(\boldsymbol{x}) :\\ \|u\|^2_{\mathcal{H}^s(\mathbb{R}^d)} = \sum\nolimits_{\substack{l\in\mathbb{N}_0^d,\\ \boldsymbol{j}\in\mathbb{Z}^d}} \lambda(\boldsymbol{l})^{2s}\cdot|u_{\boldsymbol{l},\boldsymbol{j}}|^2 \le c^2 < \infty\Big\},\end{aligned} \tag{14}$$

where $u_{\boldsymbol{l},\boldsymbol{j}} = \int_{\mathbb{R}^d} \psi^*_{\boldsymbol{l},\boldsymbol{j}}(\boldsymbol{x})u(\boldsymbol{x})d\vec{\boldsymbol{x}}$ and c is a constant which depends on d.

Based on the given one-particle basis (12) we now define a basis for many-particle spaces on $\mathbb{R}^{d\cdot N}$. We then have the $d \cdot N$-dimensional coordinates $\vec{\boldsymbol{x}} := (\boldsymbol{x}_1, \ldots, \boldsymbol{x}_N)$ where $\boldsymbol{x}_i \in \mathbb{R}^d$. To this end, we first employ a tensor product construction and define the multi-indices $\vec{\boldsymbol{l}} = (\boldsymbol{l}_1, ..., \boldsymbol{l}_N) \in \mathbb{N}_0^{d\cdot N}$ and the associated multivariate wavelets

$$\psi_{\vec{\boldsymbol{l}},\vec{\boldsymbol{j}}}(\vec{\boldsymbol{x}}) := \prod_{p=1}^{N} \psi_{\boldsymbol{l}_p,\boldsymbol{j}_p}(\boldsymbol{x}_p) = \Big(\bigotimes_{p=1}^{N} \psi_{\boldsymbol{l}_p,\boldsymbol{j}_p}\Big)(\boldsymbol{x}_1, \ldots, \boldsymbol{x}_N). \tag{15}$$

Note again that this product may involve both father and mother wavelets depending on the values of the components of the level index $\vec{\boldsymbol{l}}$. The wavelets $\psi_{\vec{\boldsymbol{l}},\vec{\boldsymbol{j}}}$ span the

subspaces $W_{\vec{l},\vec{j}} := \operatorname{span}\{\psi_{\vec{l},\vec{j}}\}$ whose union forms[3] the space

$$V = \bigoplus_{\substack{\vec{l}\in\mathbb{N}_0^{dN} \\ \vec{j}\in\mathbb{Z}^{dN}}} W_{\vec{l},\vec{j}}. \tag{16}$$

We then can uniquely represent any function u from V as

$$u(\vec{x}) = \sum_{\substack{\vec{l}\in\mathbb{N}_0^{dN} \\ \vec{j}\in\mathbb{Z}^{dN}}} u_{\vec{l},\vec{j}}\ \psi_{\vec{l},\vec{j}}(\vec{x}) \tag{17}$$

with coefficients $u_{\vec{l},\vec{j}} = \int_{\mathbb{R}^{dN}} \psi^*_{\vec{l},\vec{j}}(\vec{x})u(\vec{x})d\vec{x}$.

Now, starting from the one-particle space $\mathcal{H}^s(\mathbb{R}^d)$ we build Sobolev spaces for many particles. Obviously there are many possibilities to generalize the concept of Sobolev spaces [1] from the one-particle case to higher dimensions. Two simple possibilities are the additive or multiplicative combination i.e. an arithmetic or geometric averaging of the scales for the different particles. We use the following definition that combines both possibilities. We denote

$$\lambda_{\text{mix}}(\vec{l}) := \prod_{p=1}^{N} \lambda(\boldsymbol{l}_p) \quad \text{and} \quad \lambda_{\text{iso}}(\vec{l}) := \sum_{p=1}^{N} \lambda(\boldsymbol{l}_p). \tag{18}$$

Now, for $-\infty < t, r < \infty$, set

$$\begin{aligned} &\mathcal{H}^{t,r}_{\text{mix}}((\mathbb{R}^d)^N) \\ &\quad = \Big\{u(\vec{x}) = \textstyle\sum_{\substack{\vec{l}\in\mathbb{N}_0^{dN} \\ \vec{j}\in\mathbb{Z}^{dN}}} u_{\vec{l},\vec{j}}\psi_{\vec{l},\vec{j}}(\vec{x}) : \\ &\qquad \|u\|^2_{\mathcal{H}^{t,r}_{\text{mix}}((\mathbb{R}^d)^N)} = \textstyle\sum_{\vec{l}\in\mathbb{N}_0^{dN}} \lambda_{\text{mix}}(\vec{l})^{2t} \cdot \lambda_{\text{iso}}(\vec{l})^{2r} \cdot \sum_{\vec{j}\in\mathbb{Z}^{dN}} |u_{\vec{l},\vec{j}}|^2 \le c^2 < \infty\Big\} \end{aligned} \tag{19}$$

with a constant c which depends on d and N.

The standard isotropic Sobolev spaces [1] as well as the Sobolev spaces of dominating mixed smoothness [58], both generalized to the N-particle case, are included here. They can be written as the special cases

$$\mathcal{H}^s((\mathbb{R}^d)^N) = \mathcal{H}^{0,s}_{\text{mix}}((\mathbb{R}^d)^N) \quad \text{and} \quad \mathcal{H}^t_{\text{mix}}((\mathbb{R}^d)^N) = \mathcal{H}^{t,0}_{\text{mix}}((\mathbb{R}^d)^N),$$

respectively. Hence, the parameter r from (19) governs the isotropic smoothness, whereas t governs the mixed smoothness. Thus, the spaces $\mathcal{H}^{t,r}_{\text{mix}}$ give us a quite flexible framework for the study of problems in Sobolev spaces. Note that the relations $\mathcal{H}^t_{\text{mix}} \subset \mathcal{H}^t \subset \mathcal{H}^{t/N}_{\text{mix}}$ for $t \ge 0$ and $\mathcal{H}^{t/N}_{\text{mix}} \subset \mathcal{H}^t \subset \mathcal{H}^t_{\text{mix}}$ for $t \le 0$ hold. See [58] and [36] for more information on the spaces $\mathcal{H}^t_{\text{mix}}$.

[3] Except for the completion with respect to a chosen Sobolev norm, V is just the associated Sobolev space.

4. Semidiscrete general sparse grid spaces

We now consider truncation of the series expansion (17) with respect to the level parameter $\vec{l}$ but keep the part of the full series expansion with respect to the position parameter $\vec{j}$. To this end, we introduce, besides the parameter L (after proper scaling with c) which indicates the truncation of the scale with respect to the one-particle space, an additional parameter $T \in (-\infty, 1]$ which regulates the truncation pattern for the interaction between particles. We define the generalized sparse grid space

$$V_{L,T} := \bigoplus_{\vec{l} \in \Omega_{L,T}} W_{\vec{l}} \quad \text{where } W_{\vec{l}} = \text{span}\{\psi_{\vec{l},\vec{j}}, \vec{j} \in \mathbb{Z}^{dN}\} \tag{20}$$

with associated generalized hyperbolic cross with respect to the scale-parameter $\vec{l}$

$$\Omega_{L,T} := \{\vec{l} \in \mathbb{N}_0^{d \cdot N} : \lambda_{\text{mix}}(\vec{l}) \cdot \lambda_{\text{iso}}(\vec{l})^{-T} \leq (2^L)^{1-T}\}. \tag{21}$$

The parameter T allows us to switch from the full grid case $T = -\infty$ to the conventional sparse grid case $T = 0$, compare [12], [31], [42], and also allows to create with $T \in (0, 1]$ subspaces of the hyperbolic cross/conventional sparse grid space. Obviously, the inclusions $V_{L,T_1} \subset V_{L,T_2}$ for $T_1 \leq T_2$ hold. Figure 3 displays the index sets for various choices of T for the case $d = 1$, $N = 2$ and $L = 128$.

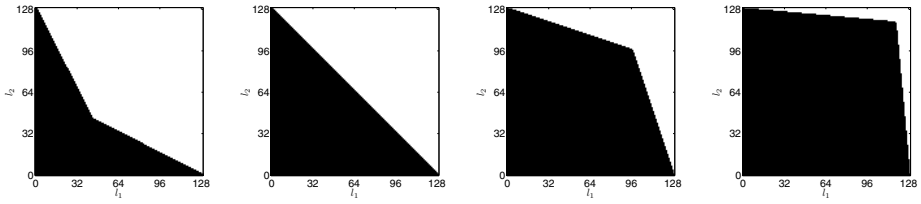

Figure 3. $\Omega_{128,T}$ for $T = 0.5, 0, -2, -10$ (from left to right), $d = 1$, $N = 2$; the conventional sparse grid/hyperbolic cross corresponds to $T = 0$. For $T = -\infty$ we get a completely black square.

We then can uniquely represent any function u from $V_{K,T}$ as

$$u(\vec{x}) = \sum_{\vec{l} \in \Omega_{L,T}, \vec{j} \in \mathbb{Z}^{d \cdot N}} u_{\vec{l},\vec{j}} \; \psi_{\vec{l},\vec{j}}(\vec{x}).$$

Such a projection into $V_{K,T}$ introduces an error. Here we have the following error estimate:

Lemma 1. *Let $s < r + t, t \geq 0$, $u \in \mathcal{H}^{t,r}_{\text{mix}}((\mathbb{R}^d)^N)$. Let $\tilde{u}_{L,T}$ be the best approximation in $V_{L,T}$ with respect to the $\mathcal{H}^s$-norm and let $u_{L,T}$ be the interpolant of u in*

$V_{L,T}$, *i.e.* $u_{L,T} = \sum_{\vec{l} \in \Omega_{L,T}} \sum_{\vec{j} \in \mathbb{Z}^{dN}} u_{\vec{l},\vec{j}} \psi_{\vec{l},\vec{j}}(\vec{x})$. *Then, there holds*

$$\inf_{V_{L,T}} \|u - v\|_{\mathcal{H}^s} = \|u - \tilde{u}_{L,T}\|_{\mathcal{H}^s} \leq \|u - u_{L,T}\|_{\mathcal{H}^s} \leq \begin{cases} O((2^L)^{s-r-t+(Tt-s+r)\frac{N-1}{N-T}}) \cdot \|u\|_{\mathcal{H}^{t,r}_{\mathrm{mix}}} & \text{for } T \geq \frac{s-r}{t}, \\ O((2^L)^{s-r-t}) \cdot \|u\|_{\mathcal{H}^{t,r}_{\mathrm{mix}}} & \text{for } T \leq \frac{s-r}{t}. \end{cases} \quad (22)$$

For a proof, compare the arguments in [31], [42], [43], [30]. This type of estimate was already given for the case of a dyadically refined wavelet basis with $d = 1$ for the periodic case on a finite domain in [31], [42], [43]. It is a generalization of the energy-norm based sparse grid approach of [11], [12], [29] where the case $s = 1$, $t = 2$, $r = 0$ was considered using a hierarchical piecewise linear basis.

Let us discuss some cases. For the standard Sobolev space $\mathcal{H}^{0,r}_{\mathrm{mix}}$ (i.e. $t = 0$, $r = 2$) and the spaces $V_{L,T}$ with $T \geq -\infty$ the resulting order is dependent of T and dependent on the number of particles N. In particular the order even deteriorates with larger T. For the standard Sobolev spaces of bounded mixed derivatives $\mathcal{H}^{t,0}_{\mathrm{mix}}$ (i.e. $t = 2$, $r = 0$) and the spaces $V_{L,T}$ with $T > \frac{s}{2}$ the resulting order is dependent of T and dependent on the number of particles N whereas for $T \leq \frac{s}{2}$ the resulting order is independent of T and N. If we restrict the class of functions for example to $\mathcal{H}^{1,1}_{\mathrm{mix}}$ (i.e. $t = 1$, $r = 1$) and measure the error in the $\mathcal{H}^1$-norm (i.e. $s = 1$) the approximation order is dependent on N for all $T > 0$ and independent on N and T for all $T \leq 0$. Note that in all cases the constants in the O-notation depend on N and d.

5. Antisymmetric semidiscrete general sparse grid spaces

Let us now come back to the Schrödinger equation (1). Note that in general an electronic wave function depends in addition to the positions $\boldsymbol{x}_i$ of the electrons also on their associated spin coordinates $\sigma_i \in \{-\frac{1}{2}, \frac{1}{2}\}$. Thus electronic wave functions are defined as $\Psi\colon (\mathbb{R}^d)^N \times \{-\frac{1}{2}, \frac{1}{2}\}^N \to \mathbb{R}\colon (\vec{x}, \vec{\sigma}) \to \Psi(\vec{x}, \vec{\sigma})$ with spin coordinates $\vec{\sigma} = (\sigma_1, \ldots, \sigma_N)$. Furthermore, physically relevant eigenfunctions Ψ obey the following two assumptions: First, elementary particles are indistinguishable from each other (fundamental principle of quantum mechanics). Second, no two electrons may occupy the same quantum state simultaneously (Pauli exclusion principle). Thus, we consider only wave functions which are antisymmetric with respect to an arbitrary simultaneous permutation $P \in \mathcal{S}_N$, of the electron positions and spin variables, i.e. which fulfil

$$\Psi(P\vec{x}, P\vec{\sigma}) = (-1)^{|P|} \Psi(P\vec{x}, P\vec{\sigma}).$$

Here $\mathcal{S}_N$ is the symmetric group. The permutation P is a mapping $P\colon \{1, \ldots, N\} \to \{1, \ldots, N\}$ which translates to a permutation of the corresponding numbering of

electrons and thus to a permutation of indices, i.e. we have $P(\boldsymbol{x}_1, \ldots, \boldsymbol{x}_N)^T := (\boldsymbol{x}_{P(1)}, \ldots, \boldsymbol{x}_{P(N)})^T$ and $P(\sigma_1, \ldots, \sigma_N)^T := (\sigma_{P(1)}, \ldots, \sigma_{P(N)})^T$. In particular, the symmetric group is of size $|\mathcal{S}_N| = N!$ and the expression $(-1)^{|P|}$ is equal to the determinant $\det P$ of the associated permutation matrix.

Now, to a given spin vector $\vec{\sigma} \in \left\{-\frac{1}{2}, \frac{1}{2}\right\}^N$ we define the associated spatial component of the full wave function Ψ by $\Psi_{\vec{\sigma}}\colon (\mathbb{R}^d)^N \to \mathbb{R}\colon \vec{\boldsymbol{x}} \to \Psi(\vec{\boldsymbol{x}}, \vec{\sigma})$. Then, since there are 2^N possible different spin distributions $\vec{\sigma}$, the full Schrödinger equation, i.e. the eigenvalue problem $H\Psi = E\Psi$, decouples into 2^N eigenvalue problems for the 2^N associated spatial components $\Psi_{\vec{\sigma}}$. Here, the spatial part $\Psi_{\vec{\sigma}}$ to a given $\vec{\sigma}$ obeys the condition

$$\Psi_{\vec{\sigma}}(P\vec{\boldsymbol{x}}) = (-1)^{|P|}\Psi_{\vec{\sigma}}(P\vec{\boldsymbol{x}}) \quad \text{for all } P \in \mathcal{S}_{\vec{\sigma}} := \{P \in \mathcal{S}_N \,:\, P\vec{\sigma} = \vec{\sigma}\}. \tag{23}$$

In particular, the minimal eigenvalue of all eigenvalue problems for the spatial components is equal to the minimal eigenvalue of the full eigenvalue problem. Moreover, the eigenfunctions of the full system can be composed by the eigenfunctions of the eigenvalue problems for the spatial parts.

Although there are 2^N possible different spin distributions $\vec{\sigma}$, the bilinear form $\langle \Psi(P\cdot)|H|\Psi(P\cdot)\rangle$ is invariant under all permutations $P \in \mathcal{S}_N$ of the position coordinates $\vec{\boldsymbol{x}}$. Thus it is sufficient to consider the eigenvalue problems which are associated to the spin vectors $\vec{\sigma}^{(N,S)} = (\sigma_1^{(N,S)}, \ldots, \sigma_N^{(N,S)})$ where the first S electrons possess spin $-\frac{1}{2}$ and the remaining $N - S$ electrons possess spin $\frac{1}{2}$, i.e.

$$\sigma_j^{(N,S)} = \begin{cases} -\frac{1}{2} & \text{for } j \le S, \\ \frac{1}{2} & \text{for } j > S. \end{cases}$$

In particular, it is enough to solve only the $\lfloor N/2 \rfloor$ eigenvalue problems which correspond to the spin vectors $\vec{\sigma}^{(N,S)}$ with $S \le N/2$. For further details see [66]. Therefore, we consider in the following without loss of generality only spin distributions $\vec{\sigma}^{(N,S)} = (\sigma_1^{(N,S)}, \ldots, \sigma_N^{(N,S)})$. We set $\mathcal{S}_{(N,S)} := \mathcal{S}_{\vec{\sigma}^{(N,S)}}$. Note that there holds $|\mathcal{S}_{(N,S)}| = S!(N-S)!$.

Now we define spaces of antisymmetric functions and their semi-discrete sparse grid counterparts. The functions of the N-particle space V from (16) which obey the anti-symmetry condition (23) for a given $\vec{\sigma}^{(N,S)}$ form a linear subspace $V^{\mathcal{A}^{(N,S)}}$ of V. We define the projection into this subspace, i.e. the antisymmetrization operator $\mathcal{A}^{(N,S)}\colon V \to V^{\mathcal{A}^{(N,S)}}$ by

$$\mathcal{A}^{(N,S)}u(\vec{\boldsymbol{x}}) := \frac{1}{S!(N-S)!} \sum_{P \in \mathcal{S}_{N,S}} (-1)^{|P|} u(P\vec{\boldsymbol{x}}). \tag{24}$$

For any basis function $\psi_{\vec{l},\vec{j}}$ of our general N-particle space V we then have

$$\begin{aligned}
\mathcal{A}^{(N,S)}\psi_{\vec{l},\vec{j}}(\vec{x}) &= \mathcal{A}^{(N,S)}\Big(\Big(\bigotimes_{p=1}^{S}\psi_{l_p,j_p}\Big)(x_1,\ldots,x_S)\Big(\bigotimes_{p=S+1}^{N}\psi_{l_p,j_p}\Big)(x_{S+1},\ldots x_N)\Big)\\
&= \Big(\mathcal{A}^{(S,S)}\bigotimes_{p=1}^{S}\psi_{l_p,j_p}(x_1,\ldots,x_S)\Big)\Big(\mathcal{A}^{(N-S,N-S)}\bigotimes_{p=S+1}^{N}\psi_{l_p,j_p}(\vec{x}_{S+1},\ldots,x_N)\Big)\\
&= \Big(\frac{1}{S!}\bigwedge_{p=1}^{S}\psi_{l_p,j_p}\Big(x_1,\ldots,x_S\Big)\Big)\Big(\frac{1}{(N-S)!}\bigwedge_{p=S+1}^{N}\psi_{l_p,j_p}\Big(x_{S+1},\ldots,x_N\Big)\Big)\\
&= \frac{1}{S!(N-S)!}\sum_{P\in\mathcal{S}_{N,S}}(-1)^{|P|}\psi_{\vec{l},\vec{j}}(P\vec{x}) = \frac{1}{S!(N-S)!}\sum_{P\in\mathcal{S}_{N,S}}(-1)^{|P|}\psi_{P\vec{l},P\vec{j}}(\vec{x}).
\end{aligned}$$

In other words, the classical product

$$\psi_{\vec{l},\vec{j}}(\vec{x}) := \prod_{p=1}^{N}\psi_{l_p,j_p}(x_p) = \Big(\bigotimes_{p=1}^{N}\psi_{l_p,j_p}\Big)(x_1,\ldots,x_N)$$

gets replaced by the product of two outer products

$$\frac{1}{S!}\bigwedge_{p=1}^{S}\psi_{l_p,j_p}(x_1,\ldots,x_S) \quad\text{and}\quad \frac{1}{(N-S)!}\bigwedge_{p=S+1}^{N}\psi_{l_p,j_p}(x_{S+1},\ldots,x_N)$$

that correspond to the two sets of coordinates and one-particle bases which are associated to the two spin values $-\frac{1}{2}$ and $\frac{1}{2}$. The outer product involves just the so-called slater determinant [55], i.e.

$$\bigwedge_{p=1}^{N}\psi_{l_p,j_p}(x_1,\ldots,x_N) = \begin{vmatrix}\psi_{l_1,j_1}(x_1) & \ldots & \psi_{l_1,j_1}(x_N)\\ \vdots & \ddots & \vdots\\ \psi_{l_N,j_N}(x_1) & \ldots & \psi_{l_N,j_N}(x_N)\end{vmatrix}.$$

Note here again that due to (11) both father wavelet functions and mother wavelet functions may be involved in the respective products.

The sequence $\{\mathcal{A}^{(N,S)}\psi_{\vec{l},\vec{j}}\}_{\vec{l}\in\mathbb{N}_0^{dN},\vec{j}\in\mathbb{Z}^{dN}}$ only forms a generating system of the antisymmetric subspace $V^{\mathcal{A}^{(N,S)}}$ and no basis since many functions $\mathcal{A}^{(N,S)}\psi_{\vec{l},\vec{j}}$ are identical (up to the sign). But we can gain a basis for the antisymmetric subspace $V^{\mathcal{A}^{(N,S)}}$ if we restrict the sequence $\{\mathcal{A}^{(N,S)}\psi_{\vec{l},\vec{j}}\}_{\vec{l}\in\mathbb{N}_0^{dN},\vec{j}\in\mathbb{Z}^{dN}}$ properly. This can be done in many different ways. A possible orthonormal basis $\mathcal{B}^{(N,S)}$ for $V^{\mathcal{A}^{(N,S)}}$ is given with help of

$$\Phi^{(N,S)}_{\vec{l},\vec{j}}(\vec{x}) := \frac{1}{\sqrt{S!(N-S)!}}\cdot\bigwedge_{p=1}^{S}\psi_{l_p,j_p}(x_1,\ldots,x_S)\cdot\bigwedge_{p=S+1}^{N}\psi_{l_p,j_p}(x_{S+1},\ldots,x_N) \tag{25}$$

as follows:

$$\mathcal{B}^{(N,S)} := \big\{\Phi^{(N,S)}_{\vec{l},\vec{j}} : \vec{l} \in \mathbb{N}_0^{d\cdot N},\ \vec{j} \in \mathbb{Z}^{d\cdot N},\ (\boldsymbol{l}_1, \boldsymbol{j}_1) < \cdots < (\boldsymbol{l}_S, \boldsymbol{j}_S) \text{ and } (\boldsymbol{l}_{S+1}, \boldsymbol{j}_{S+1}) < \cdots < (\boldsymbol{l}_N, \boldsymbol{j}_N)\big\} \tag{26}$$

where for the index pair

$$\boldsymbol{I}_p := (\boldsymbol{l}_p, \boldsymbol{j}_p) = (\boldsymbol{l}_{p,(1)}, \ldots, \boldsymbol{l}_{p,(d)}, \boldsymbol{j}_{p,(1)}, \ldots, \boldsymbol{j}_{p,(d)})$$

the relation $<$ is defined as

$$\boldsymbol{I}_p < \boldsymbol{I}_q \quad \Longleftrightarrow \quad \begin{array}{l}\text{there exists } \alpha \in \{1, \ldots, 2d\} \text{ such that } \boldsymbol{I}_{p,(\alpha)} < \boldsymbol{I}_{q,(\alpha)} \\ \text{and } \boldsymbol{I}_{p,(\beta)} \le \boldsymbol{I}_{q,(\beta)} \text{ for all } \beta \in \{1, \ldots, \alpha - 1\}.\end{array}$$

With

$$\Omega^{\mathcal{A}^{(N,S)}} = \{(\vec{l}, \vec{j}) : \vec{l} \in \mathbb{N}_0^{d\cdot N},\ \vec{j} \in \mathbb{Z}^{d\cdot N},\ (\boldsymbol{l}_1, \boldsymbol{j}_1) < \cdots < (\boldsymbol{l}_S, \boldsymbol{j}_S) \text{ and } (\boldsymbol{l}_{S+1}, \boldsymbol{j}_{S+1}) < \cdots < (\boldsymbol{l}_N, \boldsymbol{j}_N)\big\}$$

we then can define the antisymmetric subspace $V^{\mathcal{A}^{(N,S)}}$ of V as

$$V^{\mathcal{A}^{(N,S)}} = \bigoplus_{(\vec{l},\vec{j})\in\Omega^{\mathcal{A}^{(N,S)}}} W_{\vec{l},\vec{j}} \tag{27}$$

where we denote from now on $W_{\vec{l},\vec{j}} = \operatorname{span}\{\Phi^{(N,S)}_{\vec{l},\vec{j}}(\vec{x})\}$. Any function u from $V^{\mathcal{A}^{(N,S)}}$ can then uniquely be represented as

$$u(\vec{x}) = \sum_{(\vec{l},\vec{j})\in\Omega^{\mathcal{A}^{(N,S)}}} u_{\vec{l},\vec{j}}\ \Phi^{(N,S)}_{\vec{l},\vec{j}}(\vec{x})$$

with coefficients $u_{\vec{l},\vec{j}} = \int_{I^{dN}} \Phi^{(N,S)*}_{\vec{l}\vec{j}}(\vec{x}) u(\vec{x}) d\vec{x}$.

Now we are in the position to consider semidiscrete subspaces of $V^{\mathcal{A}^{(N,S)}}$. To this end, in analogy to (20) we define the generalized semidiscrete antisymmetric sparse grid spaces

$$V^{\mathcal{A}^{(N,S)}}_{L,T} := \bigoplus_{(\vec{l},\vec{j})\in\Omega^{\mathcal{A}^{(N,S)}}_{K,T}} W_{\vec{l},\vec{j}}$$

with associated antisymmetric generalized sets

$$\Omega^{\mathcal{A}^{(N,S)}}_{L,T} := \{(\vec{l}, \vec{j}) : \vec{l} \in \mathbb{N}_0^{d\cdot N},\ \vec{j} \in \mathbb{Z}^{d\cdot N},\ \lambda_{\text{mix}}(\vec{l}) \cdot \lambda_{\text{iso}}(\vec{l})^{-T} \le (2^L)^{1-T},\ (\boldsymbol{l}_1, \boldsymbol{j}_1) < \cdots < (\boldsymbol{l}_S, \boldsymbol{j}_S) \text{ and } (\boldsymbol{l}_{S+1}, \boldsymbol{j}_{S+1}) < \cdots < (\boldsymbol{l}_N, \boldsymbol{j}_N)\}.$$

Obviously, the inclusions $V^{\mathcal{A}^{(N,S)}}_{K,T_1} \subset V^{\mathcal{A}^{(N,S)}}_{K,T_2}$ for $T_1 \le T_2$ hold. Note that for the associated error the same type of estimate as in Lemma 1 holds. The number of $\vec{l}$-subbands however, i.e. the number of subsets of indices from $\Omega^{\mathcal{A}^{(N,S)}}_{L,T}$ with the same $\vec{l}$, is reduced by the factor $S!(N-S)!$.

6. Regularity and decay properties of the solution

So far we introduced various semidiscrete sparse grid spaces for particle problems and carried these techniques over to the case of antisymmetric wave functions. Here, the order of the error estimate depended on the degree s of the Sobolev-norm in which we measure the approximation error and the degrees t and r of anisotropic and isotropic smoothness, respectively, which was assumed to hold for the continuous wave function.

We now return to the electronic Schrödinger problem (1) and invoke our general theory for this special case. To this end, let us recall a major result from [67]. There, Yserentant showed with the help of Fourier transforms that an antisymmetric solution of the electronic Schrödinger equation with $d = 3$ possesses $\mathcal{H}^{1,1}_{\text{mix}}$-regularity in the case $S = 0$ or $S = N$ and at least $\mathcal{H}^{1/2,1}_{\text{mix}}$-regularity otherwise. The main argument to derive this fact is a Hardy type inequality, see [67] for details.

Let us first consider the case of a full antisymmetric solution, i.e. the case $S = 0$ or $S = N$, and the resulting approximation rate in more detail. If we measure the approximation error in the $\mathcal{H}^1$-norm, we obtain from Lemma 1 with $s = 1$ and $t = r = 1$ the approximation order $O((2^L)^{-1+T\cdot\frac{N-1}{N-T}})$ for $T \geq 0$ and $O(2^{-L})$ for $T \leq 0$. In particular, for the choice $T = 0$ we have a rate of $O(2^{-L})$. Also note that the constant in the estimate still depends on N and d.

In an analog way we can argue for the partial antisymmetric case where we have for an arbitrary chosen $1 \leq S \leq N$ at least $\mathcal{H}^{1/2,1}_{\text{mix}}$-regularity of the associated wave function. If we measure the approximation error in the $\mathcal{H}^1$-norm, we obtain from Lemma 1 with $s = 1$ and $t = 1/2$, $r = 1$ ($\mathcal{H}^{1/2,1}_{\text{mix}}$-regularity) the approximation order $O((2^{L/2})^{-1+T\cdot\frac{N-1}{N-T}})$ for $T \geq 0$ and $O(2^{-L/2})$ for $T \leq 0$. In particular, for the choice $T = 0$ we have a rate of $O(2^{-L/2})$.

Note however that the order constant depends on N and d. Moreover, also the $\mathcal{H}^{1,1}_{\text{mix}}$- and $\mathcal{H}^{1/2,1}_{\text{mix}}$-terms may grow exponentially with the number N of electrons. This is a serious problem for any further discretization in $\vec{j}$-space since to compensate for this exponential growth, the parameter L has to be chosen dependent on N. Such a behavior could be seen in the case of a finite domain with periodic boundary conditions with Fourier bases from the results of the numerical experiments in [30] and was one reason why problems with higher numbers of electrons could not be treated.

In [69], a rescaling of the mixed Sobolev norm is suggested. To this end, a scaled analog of the $\mathcal{H}^{1,r}_{\text{mix}}$-norm, $r \in \{0, 1\}$, albeit in Fourier space notation (one $\vec{k}$-scale in Fourier space only instead of the $\vec{l}$- and $\vec{j}$-scales in wavelet space) is introduced, compare also [30], via

$$\|\Psi\|_{\mathcal{H}^{1,r}_{\text{mix}}} = \int_{\mathbb{R}^{dN}} \Big(\prod_{p\in I}\Big(1+\Big|\frac{\boldsymbol{k}_p}{R}\Big|^2\Big)\Big)\Big(\sum_{p=1}^{N}\Big|\frac{\boldsymbol{k}_p}{R}\Big|^2\Big)^r |\hat{\Psi}(\vec{\boldsymbol{k}})|^2 d\vec{\boldsymbol{k}} \tag{28}$$

where I denotes the subset of indices of electrons with the same spin, $\hat{\Psi}(\vec{\boldsymbol{k}})$ is the

Fourier transform of Ψ and $\vec{\boldsymbol{k}} \in \mathbb{Z}^{dN}$ are the coordinates in Fourier space with single-particle-components $\boldsymbol{k}_p \in \mathbb{R}^d$. Here the scaling parameter R relates to the intrinsic length scale of the atom or molecule under consideration. It must hold $R \leq C\sqrt{N}\max(N, Z)$ with $Z = \sum_q Z_q$ the totals charge of the nuclei, see also [56], [69]. For an electronically neutral system $Z = N$ and thus $R \leq CN^{3/2}$. Compared to our definitions λ_{mix} and λ_{iso} of (18) we see the following difference: Besides that (28) involves integration instead of summation, (28) deals with the non-octavized case whereas we used the octavized version which involves powers of two. This is one reason why in the product $\prod_{p\in I}(1 + |\boldsymbol{k}_p/R|^2)$ the factor one must be present. Otherwise the case $\boldsymbol{k}_p = \boldsymbol{0}$ is not dealt properly with. But this also opens the possibility to treat the coordinates with values zero differently in the scaling, since the scaling with $1/R$ in the product acts only on the coordinates with non-zero values.

Furthermore, with I_+ and I_- the sets of indices p of electrons for which the spin attains the values $-1/2$ and $1/2$, respectively, and a parameter K (non-octavized case), the subdomain

$$H^Y_{R,K} := \left\{(\boldsymbol{k}_1, \ldots \boldsymbol{k}_N) \in (\mathbb{R}^3)^N : \prod_{p\in I_+}\left(1 + \left|\frac{\boldsymbol{k}_p}{R}\right|_2^2\right) + \prod_{p\in I_-}\left(1 + \left|\frac{\boldsymbol{k}_p}{R}\right|_2^2\right) \leq K^2\right\} \tag{29}$$

in Fourier space describes a cartesian product of two scaled hyperbolic crosses. In the extreme cases $S = 0$ or $S = N$ it degenerates to just one hyperbolic cross. Then, with the projection

$$(P_{R,K}\Psi)(x) = \left(\frac{1}{\sqrt{2\pi}}\right)^{3N} \int \hat{\chi}_{R,K}(\vec{\boldsymbol{k}})\hat{\Psi}(\vec{\boldsymbol{k}})e^{i\vec{\boldsymbol{k}}\cdot\vec{\boldsymbol{x}}}d\vec{\boldsymbol{k}},$$

where $\hat{\chi}_{R,K}$ is the characteristic function of the domain $H^Y_{R,K}$, the following error estimate is shown in [69]: For all eigenfunctions with negative eigenvalues and $s = 0, 1$ there holds

$$\|\Psi - P_{R,K}\Psi\|_s \leq \frac{2\sqrt{e}}{K} R^s \|\Psi\|_0. \tag{30}$$

The restriction to eigenfunctions of the Schrödinger–Hamiltonian whose associated eigenvalues are strictly smaller than zero is not a severe issue since such an assumption holds for bounded states, i.e. any system with localized electrons, compare also [25], [38], [59].

This surprising result shows that, with proper scaling in the norms and the associated choice of a scaled hyperbolic cross, it is possible to get rid of the $\|\Psi\|_{\mathcal{H}^{1,r}_{\text{mix}}}$-terms on the right hand side of sparse grid estimates of the type (22). Note that these terms may grow exponentially with N whereas $\|\Psi\|_0 = 1$. To derive semidiscrete approximation spaces which, e.g. after scaling, overcome this problem is an important step towards any efficient discretization for problems with higher numbers of electrons N. Note however that e.g. already for the most simple case $S = 0$ or $S = N$ where in (29) only one cross is involved due to $I_- = \{\,\}$ or $I_+ = \{\,\}$, the subdomain $H^Y_{R,K}$ is no longer a conventional hyperbolic cross in Fourier space. Now, depending of

the different dimensions, the "rays" of the cross are chopped off due to the rescaling with R. This gets more transparent if we use the relation

$$\prod_{p=1}^{N}(1+|\boldsymbol{k}_p|_2^2) = \sum_{p=0}^{N}\sum_{\substack{a\subset\{1,\ldots,N\}\\|a|=p}}\prod_{j\in\alpha}|\boldsymbol{k}_j|_2^2$$

and rewrite (29) e.g. in the case $S=0$ or $S=N$ as

$$H_{R,K}^{Y} = \big\{\vec{\boldsymbol{k}} \,:\, K^{-2}\big(\textstyle\sum_{p=0}^{N}\sum_{\substack{a\subset\{1,\ldots,N\}\\|a|=p}} R^{-2p}\prod_{j\in\alpha}|\boldsymbol{k}_j|_2^2\big) \le 1\big\}. \tag{31}$$

If we now define for $K_0, K_1, \ldots, K_N \in \mathbb{N}$

$$H_{K_0,K_1,\ldots,K_N} := \big\{\vec{\boldsymbol{k}} \,:\, \big(\textstyle\sum_{p=0}^{N}\sum_{\substack{a\subset\{1,\ldots,N\}\\|a|=p}} K_p^{-2}\prod_{j\in\alpha}|\boldsymbol{k}_j|_2^2\big) \le 1\big\} \tag{32}$$

we have

$$H_{R^0K,R^1K,\ldots,R^NK} = H_{R,K}^{Y}$$

and see more clearly how the scaling with R acts individually on the different dimensional subsets of the Fourier coordinates. In Figure 4 we give in logarithmic and absolute representation the boundaries of the domains $H_{1,K}^{Y}$, $H_{R,K}^{Y}$ and H_{1,R^NK}^{Y} for $R=8$, $K=2^8$. Here we can observe how the scaled variant $H_{R,K}^{Y}$ is just embedded between the two non-scaled domains $H_{1,K}^{Y}$ and H_{1,R^NK}^{Y}. While the boundary of $H_{R,K}^{Y}$ matches in "diagonal" direction that of the huge regular sparse grid H_{1,R^NK}^{Y} this is no longer the case for the other directions.

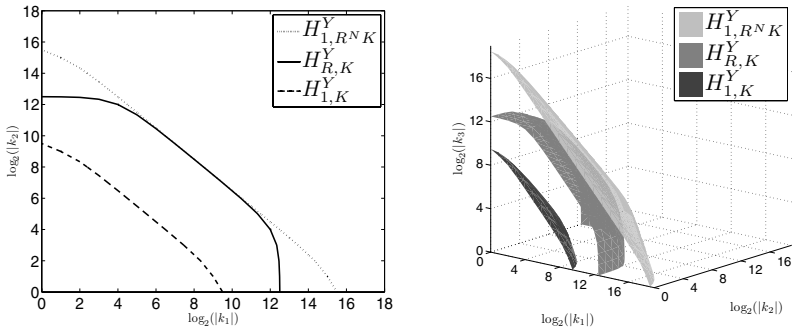

Figure 4. Sets of level indices for $H_{1,K}^{Y}$, $H_{R,K}^{Y}$, H_{1,R^NK}^{Y} in the case $d=1$, $R=8$, $K=2^8$ for $N=2$ and $N=3$.

This dimensional scaling is closely related to well-known decay properties of the solution of Schrödinger's equation which we now recall from the literature. In the seminal work of Agmon [2] the $\mathcal{L}^2$-decay of the eigenfunctions of the electronic

Schrödinger–Hamiltonian of an atom with one nucleus fixed in the origin of the coordinate system is studied in detail and a characterization of the type

$$\int_{\mathbb{R}^{N\cdot d}} |\Psi(\vec{\boldsymbol{x}})|^2 e^{2(1-\varepsilon)\rho(\vec{\boldsymbol{x}})} d\vec{\boldsymbol{x}} \leq c < \infty$$

for any $\varepsilon > 0$ is given for eigenfunctions Ψ with associated eigenvalue μ below the so-called essential spectrum of H. In other words, Ψ decays in the $\mathcal{L}^2$-sense roughly like $e^{-\rho(\vec{\boldsymbol{x}})}$. Here, $\rho(\vec{\boldsymbol{x}})$ is the geodesic distance from $\vec{\boldsymbol{x}}$ to the origin in the Riemannian metric

$$d\vec{\boldsymbol{s}}^2 = (\Lambda_{I(\vec{\boldsymbol{x}})} - \mu) \sum_{i=1}^{N} 2|d\boldsymbol{x}_i|_2^2.$$

To this end, if I denotes any proper subset of $\{1, \ldots N\}$, let H_I denote the restriction of the full Hamiltonian H to the subsystem involving only the electrons associated to I and $\Lambda_I = \inf \sigma(H_I)$, $\Lambda_I = 0$ if I is empty. For any $\vec{\boldsymbol{x}} \in \mathbb{R}^{N\cdot d}/\{0\}$, $I(\vec{\boldsymbol{x}})$ denotes the subset of integers $i \in \{1, \ldots, N\}$ for which $\boldsymbol{x}_i = \boldsymbol{0}$. Note that ρ is *not* isotropic but takes at each point $\vec{\boldsymbol{x}}$ the amount of electrons with position $\boldsymbol{0}$, i.e. the number of electron-nucleus cusps into account.

The result (30) gives some hope that it might indeed be possible to find after additional discretization (in $\vec{\boldsymbol{j}}$-space) an overall discretization which is cost effective and results in an error which does not grow exponentially with the amount of electrons.

The idea is now to decompose the scaled hyperbolic cross $H^Y_{R,K}$ in Fourier space and to approximate the corresponding parts of the associated projection $P_{R,K}\hat{\Psi}(\vec{\boldsymbol{k}})$ properly. To this end, let us assume that we consider a non-periodic, isolated system. It then can be shown that any eigenfunction Ψ with negative eigenvalue below the essential spectrum of the Schrödinger operator H decays exponentially in the $\mathcal{L}^2$-sense with $|\vec{\boldsymbol{x}}| \to \infty$. The same holds for its first derivative [37]. A consequence is that the Fourier transform $\hat{\Psi}$ is infinitely often differentiable as a function in $\vec{\boldsymbol{k}}$. Let us now decompose $H^Y_{R,K}$ into finitely many subdomains $H^Y_{R,K,\vec{\boldsymbol{l}}}$ and let us split $\hat{\Psi}_{R,K}(\vec{\boldsymbol{k}}) := \hat{\chi}_{R,K}(\vec{\boldsymbol{k}})\hat{\Psi}(\vec{\boldsymbol{k}})$ accordingly into $\hat{\Psi}_{R,K,\vec{\boldsymbol{l}}}(\vec{\boldsymbol{k}})$, i.e.

$$\hat{\Psi}_{R,K}(\vec{\boldsymbol{k}}) = \sum_{\vec{\boldsymbol{l}}} \hat{\chi}_{\vec{\boldsymbol{l}}} \hat{\Psi}_{R,K}(\vec{\boldsymbol{k}}) = \sum_{\vec{\boldsymbol{l}}} \hat{\Psi}_{R,K,\vec{\boldsymbol{l}}}(\vec{\boldsymbol{k}})$$

by means of a C^∞-partition of unity $\sum_{\vec{\boldsymbol{l}}} \hat{\chi}_{\vec{\boldsymbol{l}}} = 1$ on $H^Y_{R,K}$, i.e. each $\hat{\chi}_{\vec{\boldsymbol{l}}}(\vec{\boldsymbol{k}}) \in C^\infty$ as a function in $\vec{\boldsymbol{k}}$. Then the functions $\hat{\Psi}_{R,K,\vec{\boldsymbol{l}}}(\vec{\boldsymbol{k}})$ inherit the C^∞-smoothness property and thus can each be well and efficiently approximated by e.g. a properly truncated Fourier series expansion. Note that the detailed choice of partition of unity is not yet specified and there are many possibilities. In the following we will use, e.g. after proper scaling, cf. (10) and (11), the partition

$$\hat{\chi}_{\vec{\boldsymbol{l}}}(\vec{\boldsymbol{k}}) = \prod_{p=1}^{N} \prod_{i=1}^{d} \hat{\chi}_{I_{p,(i)}}(\boldsymbol{k}_{p,(i)})$$

where

$$\hat{\chi}_l(k) := \begin{cases} \hat{\chi}(\frac{k}{c}) & \text{for } l = 0, \\ \hat{\chi}(\frac{k}{c2^l}) - \hat{\chi}(\frac{k}{c2^{l-1}}) & \text{for } l > 0, \end{cases}$$

with

$$\hat{\chi}(k) = \begin{cases} 1 & \text{for } |k| \le \frac{2\pi}{3}, \\ \cos\left(\frac{\pi}{2} \frac{e^{-\frac{4\pi^2}{(3k+2\pi)^2}}}{e^{-\frac{4\pi^2}{(4\pi+3k)^2}} + e^{-\frac{4\pi^2}{(3x+2\pi)^2}}} \right)^2 & \text{for } \frac{2\pi}{3} \le |k| \le \frac{4\pi}{3}, \\ 0 & \text{for } |k| \ge \frac{4\pi}{3}. \end{cases}$$

This choice results in just a representation with respect to the Meyer wavelet series with ν^∞, i.e. (9) with $\alpha = 2$, compare also (7). The Fourier series expansion of each $\hat{\Psi}_{R,K,\vec{l}}(\vec{k})$ then introduces just the $\vec{j}$-scale, while the $\vec{k}$-scale of the Fourier space relates to the $\vec{l}$-scale of the Meyer wavelets. All we now need is a good decomposition of $H^Y_{R,K}$ into subdomains, a choice of smooth $\hat{\chi}_{\vec{l}}$'s and a proper truncation of the Fourier series expansion of each of the $\hat{\Psi}_{R,K,\vec{l}}$'s. This corresponds to a *truncation* of the Meyer wavelet expansion of Ψ in $\mathbb{R}^{d\cdot N}$ with respect to both the $\vec{l}$- and the $\vec{j}$-scale. Presently, however, it is not completely clear what choice of decomposition and what kind of truncation of the expansion within each subband $\vec{l}$ is most favourable with respect to both the resulting number M of degrees of freedom and the corresponding accuracy of approximation for varying number N of electrons. Anyway, with the choice $K = 2^L$ the set of indices in $\vec{l}, \vec{j}$-wavelet space which is associated to (29) reads

$$\Omega^{\mathcal{A}^{(N,S)}}_{H^Y_{R,2^L}} := \Big\{ (\vec{l}, \vec{j}) \in \Omega^{\mathcal{A}^{(N,S)}} \ : \ \prod_{i=1}^{S} \left(1 + \left|\frac{\tilde{\lambda}(\boldsymbol{l}_i)}{R}\right|_2^2\right) + \prod_{i=S+1}^{N} \left(1 + \left|\frac{\tilde{\lambda}(\boldsymbol{l}_i)}{R}\right|_2^2\right) \le 2^{2L} \Big\},$$

where for $\boldsymbol{l} \in \mathbb{N}_0^d$ we define

$$\tilde{\lambda}(\boldsymbol{l}) := \min_{\boldsymbol{k} \in \mathrm{supp}(\hat{\chi}_{\boldsymbol{l}})} \{|\boldsymbol{k}|_2\}.$$

Note that this involves a kind of octavization due to the size of the support of the $\hat{\chi}_{\boldsymbol{l}}$. For example, we obtain for the Shannon wavelet $\tilde{\lambda}(\boldsymbol{l}) = |(\tilde{\lambda}_{\nu^0}(l_1), \ldots, \tilde{\lambda}_{\nu^0}(l_d))|_2$ with

$$\tilde{\lambda}_{\nu^0}(l) = \begin{cases} 0 & \text{for } l = 0, \\ c\pi 2^{l-1} & \text{otherwise.} \end{cases}$$

7. Numerical experiments

We now consider the assembly of the discrete system matrix which is associated to a generalized antisymmetric sparse grid space $V_\Lambda^{\mathcal{A}^{(N,S)}}$ with corresponding finite-dimensional set $\Omega_\Lambda^{\mathcal{A}^{(N,S)}} \subset \Omega^{\mathcal{A}^{(N,S)}}$ and basis functions $\{\Phi_{\vec{l},\vec{j}}^{(N,S)} : (\vec{l},\vec{j}) \in \Omega_\Lambda^{\mathcal{A}^{(N,S)}}\}$ with $\{\Phi_{\vec{l},\vec{j}}^{(N,S)}\}$ from (25) in a Galerkin discretization of (1). To this end, we fix $N > 0$ and $0 \le S \le N$ and omit for reasons of simplicity the indices S and N in the following.

To each pair of indices $(\vec{l},\vec{j})$, $(\vec{l}',\vec{j}')$, each from $\Omega_\Lambda^{\mathcal{A}^{(N,S)}}$, and associated functions $\Phi_{\vec{l},\vec{j}}^{(N,S)}$, $\Phi_{\vec{l}',\vec{j}'}^{(N,S)}$ we obtain one entry in the stiffness matrix, i.e.

$$A_{(\vec{l},\vec{j}),(\vec{l}',\vec{j}')} := \langle \Phi_{\vec{l},\vec{j}}^{(N,S)} | H | \Phi_{\vec{l}',\vec{j}'}^{(N,S)} \rangle = \int \Phi_{\vec{l},\vec{j}}^{(N,S)*}(\vec{x}) H \Phi_{\vec{l}',\vec{j}'}^{(N,S)}(\vec{x})\, \mathrm{d}\vec{x}. \tag{33}$$

Since we use $\mathcal{L}^2$-orthogonal one-dimensional Meyer wavelets as basic building blocks in our construction, also the one-particle basis functions are $\mathcal{L}^2$-orthogonal and we furthermore have $\mathcal{L}^2$-orthogonality of the antisymmetric many-particle basis functions $\Phi_{\vec{l},\vec{j}}^{(N,S)}(\boldsymbol{x})$. We then can take advantage of the well-known Slater–Condon rules [18], [55], [60]. Consequently, quite a few entries of the system matrix are zero and the remaining non-zero entries can be put together from the values of certain d- and $2d$-dimensional integrals. These integrals can be written in terms of the Fourier transformation of the Meyer wavelets. In case of the kinetic energy operator we obtain for $\boldsymbol{l}_\alpha, \boldsymbol{l}_\beta \in \mathbb{N}_0^d$ and $\boldsymbol{j}_\alpha, \boldsymbol{j}_\beta \in \mathbb{Z}^d$

$$\begin{aligned}\langle \psi_{\boldsymbol{l}_\alpha,\boldsymbol{j}_\alpha} | -\frac{1}{2}\Delta | \psi_{\boldsymbol{l}_\beta,\boldsymbol{j}_\beta} \rangle &= \frac{1}{2}\int_{\mathbb{R}^d} \nabla \psi^*_{\boldsymbol{l}_\alpha,\boldsymbol{j}_\alpha}(\boldsymbol{x}) \cdot \nabla \psi_{\boldsymbol{l}_\beta,\boldsymbol{j}_\beta}(\boldsymbol{x}) d\boldsymbol{x} \\ &= \frac{1}{2}\sum_{\mu=1}^{d} \int_{\mathbb{R}} k_\mu^2 \hat{\psi}^*_{\boldsymbol{l}_{\alpha,(\mu)},\boldsymbol{j}_{\alpha,(\mu)}}(k_\mu) \hat{\psi}_{\boldsymbol{l}_{\beta,(\mu)},\boldsymbol{j}_{\beta,(\mu)}}(k_\mu)\, dk_\mu \prod_{\nu\neq\mu}^{d} \delta_{\boldsymbol{l}_{\alpha,(\nu)},\boldsymbol{l}_{\beta,(\nu)}} \delta_{\boldsymbol{j}_{\alpha,(\nu)},\boldsymbol{j}_{\beta,(\nu)}}\end{aligned}$$

and for the integrals related to the d-dimensional Coulomb operator $v(\boldsymbol{x}) = 1/|\boldsymbol{x}|_2$ we can write

$$\begin{aligned}\langle \psi_{\boldsymbol{l}_\alpha,\boldsymbol{j}_\alpha} | v | \psi_{\boldsymbol{l}_\beta,\boldsymbol{j}_\beta} \rangle &= \int_{\mathbb{R}^d} \psi^*_{\boldsymbol{l}_\alpha,\boldsymbol{j}_\alpha}(\boldsymbol{x}) v(\boldsymbol{x}) \psi_{\boldsymbol{l}_\beta,\boldsymbol{j}_\beta}(\boldsymbol{x}) d\boldsymbol{x} \\ &= \int_{\mathbb{R}^d} \hat{v}(\boldsymbol{k}) (\hat{\psi}_{\boldsymbol{l}_\alpha,\boldsymbol{j}_\alpha} * \hat{\psi}_{\boldsymbol{l}_\beta,\boldsymbol{j}_\beta})(\boldsymbol{k})\, d\boldsymbol{k}.\end{aligned}$$

For $\boldsymbol{l}_\alpha, \boldsymbol{l}_\beta, \boldsymbol{l}_{\alpha'}, \boldsymbol{l}_{\beta'} \in \mathbb{N}_0^d$ and $\boldsymbol{j}_\alpha, \boldsymbol{j}_\beta, \boldsymbol{j}_{\alpha'}, \boldsymbol{j}_{\beta'} \in \mathbb{Z}^d$ we obtain the integrals related to the electron-electron operator $v(\boldsymbol{x}-\boldsymbol{y}) = 1/|\boldsymbol{x}-\boldsymbol{y}|_2$ in the form

$$\begin{aligned}&\int_{\mathbb{R}^d}\int_{\mathbb{R}^d} \psi^*_{\boldsymbol{l}_\alpha,\boldsymbol{j}_\alpha}(\boldsymbol{x}) \psi^*_{\boldsymbol{l}'_\alpha,\boldsymbol{j}_{\alpha'}}(\boldsymbol{y}) v(\boldsymbol{x}-\boldsymbol{y}) \psi_{\boldsymbol{l}_\beta,\boldsymbol{j}_\beta}(\boldsymbol{x}) \psi_{\boldsymbol{l}_{\beta'},\boldsymbol{j}_{\beta'}}(\boldsymbol{y}) d\boldsymbol{x}\, d\boldsymbol{y} \\ &\qquad = (2\pi)^{\frac{d}{2}} \int_{\mathbb{R}^d} \hat{v}(\boldsymbol{k}) (\hat{\psi}_{\boldsymbol{l}_\alpha,\boldsymbol{j}_\alpha} * \hat{\psi}_{\boldsymbol{l}_\beta,\boldsymbol{j}_\beta})(\boldsymbol{k}) (\hat{\psi}_{\boldsymbol{l}_{\alpha'},\boldsymbol{j}_{\alpha'}} * \hat{\psi}_{\boldsymbol{l}_{\beta'},\boldsymbol{j}_{\beta'}})(\boldsymbol{k})\, d\boldsymbol{k}.\end{aligned}$$

Here, $f * g$ denotes the Fourier convolution, namely $(2\pi)^{-\frac{d}{2}} \int_{\mathbb{R}^d} f(\boldsymbol{x} - \boldsymbol{y}) g(\boldsymbol{y})\, d\boldsymbol{y}$. Note that, in the case of the Meyer wavelet tensor-product basis, the d-dimensional Fourier convolution can be written in terms of the one-dimensional Fourier convolution

$$(\hat{\psi}_{\boldsymbol{l}_\alpha, \boldsymbol{j}_\alpha} * \hat{\psi}_{\boldsymbol{l}_\beta, \boldsymbol{j}_\beta})(\boldsymbol{k}) = \prod_{\mu=1}^{d} (\hat{\psi}_{l_{\alpha,(\mu)}, j_{\alpha,(\mu)}} * \hat{\psi}_{l_{\beta,(\mu)}, j_{\beta,(\mu)}})(k_\mu).$$

Thus the d-dimensional and $2d$-dimensional integrals in real space which are associated to the Coulomb operator and the electron-electron operator can be written in form of d-dimensional integrals of terms involving one-dimensional convolution integrals.

For the solution of the resulting discrete eigenvalue problem we invoke a parallelized conventional Lanczos method taken from the software package SLEPc [35] which is based on the parallel software package PETSc [6]. Note that here also other solution approaches are possible with improved complexities, like multigrid-type methods [13], [15], [44], [47] which however still need to be carried over to the setting of our generalized antisymmetric sparse grids.

Note that an estimate for the accuracy of an eigenfunction relates to an analogous estimate for the eigenvalue by means of the relation $|E - E^{\text{app}}| \leq 4 \cdot \|\Psi - \Psi^{\text{app}}\|^2_{\mathcal{L}^2}$ where E and Ψ denote the exact minimal eigenvalue and associated eigenfunction of H, respectively, and E^{app} and Ψ^{app} denote finite-dimensional Galerkin approximations in arbitrary subspaces, see also [66].

Then, with Lemma 1, we would obtain for the case $d = 3$ with $s = 0$ and, for example, $r = 1$, $t = 1$ and $S = 0$ the estimate

$$\left|E - E^{\mathcal{A}^{(N,0)}}_{L,T}\right| \leq 4 \cdot \left\|\Psi - \Psi^{\mathcal{A}^{(N,0)}}_{L,T}\right\|^2_{\mathcal{L}^2} \leq O((2^L)^{2\cdot(-2+(T+1)\frac{N-1}{N-T})}) \cdot \left\|\Psi^{\mathcal{A}^{(N,0)}}\right\|^2_{\mathcal{H}^{1,1}_{\text{mix}}}$$

and we see that the eigenvalues are in general much better approximated than the eigenfunctions. For example, for $T = 0$, this would result in a (squared) rate of the order $-4 + 2(N-1)/N$ which is about -4 for small numbers of N but gets -2 for $N \to \infty$.

Let us now describe our heuristic approach for a finite-dimensional subspace choice in wavelet space which hopefully gives us efficient a-priori patterns $\Omega^{\mathcal{A}^{(N,S)}}_{\Lambda}$ and associated subspaces $V^{\mathcal{A}^{(N,S)}}_{\Lambda}$. We use a model function of the Hylleraas-type [16], [41], [57][4]

$$h(\vec{\boldsymbol{x}}) = \prod_{p=1}^{N} \left(e^{-\alpha_p |\boldsymbol{x}_p|_2} \prod_{q>p}^{N} e^{-\beta_{p,q} |\boldsymbol{x}_p - \boldsymbol{x}_q|_2} \right) \tag{34}$$

which reflects the decay properties, the nucleus cusp and the electron-electron cusps of an atom in real space with nucleus fixed in the origin as guidance to a-priori derive a pattern of active wavelet indices in space and scale similar to the simple

[4]Note that we omitted here any prefactors for reasons of simplicity.

one-dimensional example of Figure 2. The localization peak of a Meyer wavelet $\psi_{l,j}$ in real space (e.g. after proper scaling with some c analogously to (10)) is given by

$$\theta(l, j) = \iota(l, j)2^{-l} \quad \text{where } \iota(l, j) = \begin{cases} j & \text{for } l = 0, \\ 1 + 2j & \text{otherwise,} \end{cases}$$

which leads in the multidimensional case to

$$\theta_{\vec{l},\vec{j}} = (\theta(l_1, j_1), \ldots, \theta(l_d, j_d)) \in \mathbb{R}^d$$
$$\theta_{\vec{l},\vec{j}} = (\theta(\boldsymbol{l}_1, \boldsymbol{j}_1), \ldots, \theta(\boldsymbol{l}_N, \boldsymbol{j}_N)) \in (\mathbb{R}^d)^N$$

We now are in the position to describe different discretizations with respect to both the $\vec{\boldsymbol{l}}$-scale and the $\vec{\boldsymbol{j}}$-scale. We focus with respect to the $\vec{\boldsymbol{j}}$-scale on three cases: First, we restrict the whole real space to a finite domain and take the associated wavelets on all incorporated levels into account. Note that in this case the number of wavelets grows from level to level by a factor of 2. Second, we use on each level the same prescribed fixed number of wavelets. And third we let the number of wavelets decay from level to level by a certain factor which results in a multivariate analog to the triangular subspace of Figure 2 (right). With respect to the $\vec{\boldsymbol{l}}$-scale we rely in all cases on the regular sparse grid with $T = 0$. These three different discretization approaches are illustrated in the Figures 5–8 for $d = 1$, $N = 1$ and $d = 1$, $N = 2$, respectively.

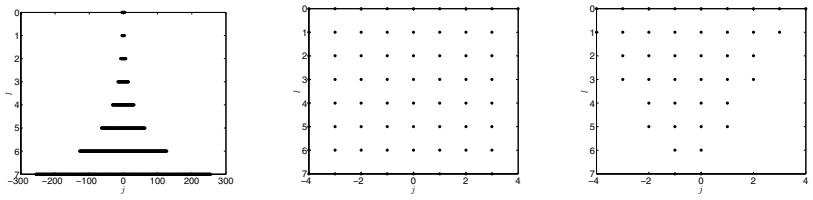

Figure 5. From left to right: Index sets $\Omega^{\mathcal{A}^{(N,S)}}_{\Lambda^{\text{full}}(L,J,R)}$, $\Omega^{\mathcal{A}^{(N,S)}}_{\Lambda^{\Theta_{\text{rec}}}(L,J,R)}$ and $\Omega^{\mathcal{A}^{(N,S)}}_{\Lambda^{\Theta_{\text{tri}}}(L,J,R)}$ with $d = 1$, $N = 1$, $L = 8$, $J = 4$, $R = 1$ and $\alpha_1 = 1$.

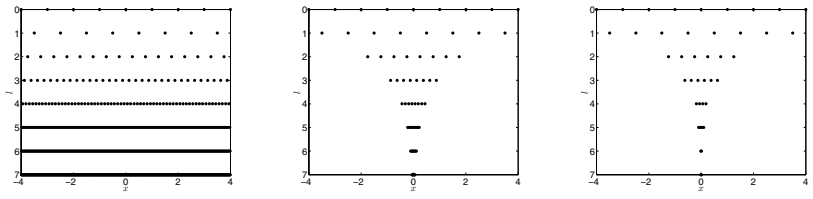

Figure 6. From left to right: Localization peaks of basis functions in real space corresponding to index sets $\Omega^{\mathcal{A}^{(N,S)}}_{\Lambda^{\text{full}}(L,J,R)}$, $\Omega^{\mathcal{A}^{(N,S)}}_{\Lambda^{\Theta_{\text{rec}}}(L,J,R)}$ and $\Omega^{\mathcal{A}^{(N,S)}}_{\Lambda^{\Theta_{\text{tri}}}(L,J,R)}$ with $d = 1$, $N = 1$, $L = 8$, $J = 4$, $R = 1$ and $\alpha_1 = 1$.

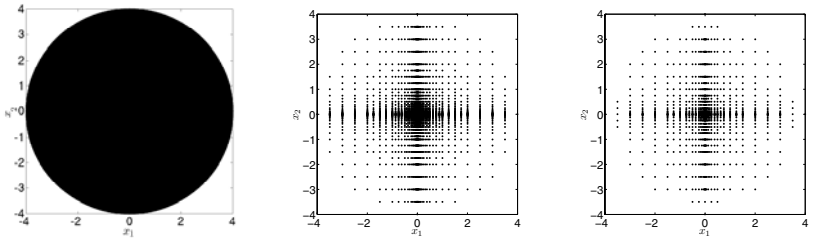

Figure 7. From left to right: Localization peaks of basis functions in real space corresponding to the index sets $\Omega^{\mathcal{A}^{(N,S)}}_{\Lambda^{\text{full}}(L,J,R)}$, $\Omega^{\mathcal{A}^{(N,S)}}_{\Lambda^{\Theta_{\text{rec}}}(L,J,R)}$ and $\Omega^{\mathcal{A}^{(N,S)}}_{\Lambda^{\Theta_{\text{tri}}}(L,J,R)}$ with $d = 2$, $N = 1$, $L = 8$, $J = 4$, $R = 1$ and $\alpha_1 = 1$.

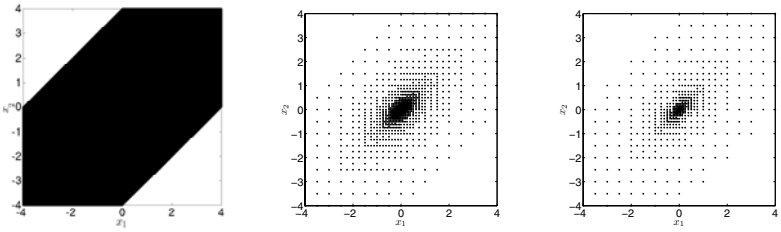

Figure 8. From left to right: Localization peaks of basis functions in real space corresponding to the index sets $\Omega^{\mathcal{A}^{(N,S)}}_{\Lambda^{\text{full}}(L,J,R)}$, $\Omega^{\mathcal{A}^{(N,S)}}_{\Lambda^{\Theta_{\text{rec}}}(L,J,R)}$ and $\Omega^{\mathcal{A}^{(N,S)}}_{\Lambda^{\Theta_{\text{tri}}}(L,J,R)}$ with $d = 1$, $N = 2$, $L = 8$, $J = 4$, $R = 1$, $S = 1$ and $\alpha_1 = \alpha_2 = \beta_{1,2} = \frac{1}{2}$.

To this end, we define with the parameter $J \in \mathbb{N}_+$ the pattern for the finite domain with full wavelet resolution, i.e. the *full* space (with respect to $\vec{\boldsymbol{j}}$-scale after a finite domain is fixed), as

$$\begin{aligned}\Omega^{\mathcal{A}^{(N,S)}}_{\Lambda^{\text{full}}(L,J,R)} &:= \left\{(\vec{\boldsymbol{l}}, \vec{\boldsymbol{j}}) \in \Omega^{\mathcal{A}^{(N,S)}}_{H^Y_{R,2^L}} : h(\theta(\vec{\boldsymbol{l}}, \vec{\boldsymbol{j}})) > e^{-J}\right\} \\ &= \left\{(\vec{\boldsymbol{l}}, \vec{\boldsymbol{j}}) \in \Omega^{\mathcal{A}^{(N,S)}}_{H^Y_{R,2^L}} : \sum_{p=1}^{N} \left(\alpha_p |\theta(\boldsymbol{l}_p, \boldsymbol{j}_p)|_2 \right.\right. \\ &\qquad \left.\left. + \sum_{q>p}^{N} \beta_{p,q} |\theta(\boldsymbol{l}_p, \boldsymbol{j}_p) - \theta(\boldsymbol{l}_q, \boldsymbol{j}_q)|_2\right) < J\right\}\end{aligned}$$

with prescribed α_p, $\beta_{p,q}$. Note here the equivalence of the sum to $\ln(h(\theta(\vec{\boldsymbol{l}}, \vec{\boldsymbol{j}})))$.

To describe the other two cases we set with a general function Θ which still has to be fixed

$$\begin{aligned}&\Omega^{\mathcal{A}^{(N,S)}}_{\Lambda^{\Theta}(L,J,R)} := \left\{(\vec{\boldsymbol{l}}, \vec{\boldsymbol{j}}) \in \Omega^{\mathcal{A}^{(N,S)}}_{\Lambda^{\text{full}}(L,J,R)} :\right. \\ &\left.\sum_{p=1}^{N} \left(\alpha_p \left|\Theta\left(\boldsymbol{l}_p, \boldsymbol{j}_p\right)\right|_2 + \sum_{q>p}^{N} \beta_{p,q} \left|\Theta\left(\theta^{-1}\left(\theta\left(\boldsymbol{l}_p, \boldsymbol{j}_p\right) - \theta\left(\boldsymbol{l}_q, \boldsymbol{j}_q\right)\right)\right)\right|_2\right) < J\right\}.\end{aligned}$$

Note that θ^{-1} denotes the inverse mapping to θ. It holds

$$\theta^{-1}\left(\theta\,(l,\,j)-\theta\left(l',\,j'\right)\right)=\begin{cases}\tilde{\iota}^{-1}(l,\,\iota(l,\,j)-\iota(l',\,j')2^{l-l'}) & \text{for } l\geq l',\\ \tilde{\iota}^{-1}(l',\,\iota(l,\,j)2^{l'-l}-\iota(l',\,j')) & \text{for } l'\geq l\end{cases}$$

where $\tilde{\iota}(l,\,j)=(l,\,\iota(l,\,j))$. We now define the *rectangular* index set $\Omega^{\mathcal{A}^{(N,S)}}_{\Lambda^{\mathrm{rec}}(L,J,R)}$ via the following choice of Θ: For $\boldsymbol{l}\in\mathbb{N}_0^d$ and $\boldsymbol{j}\in\mathbb{Z}^d$ we set

$$\Theta_{\mathrm{rec}}(\boldsymbol{l},\,\boldsymbol{j}):=(\Theta_{\mathrm{rec}}(l_1,\,j_1),\ldots,\Theta_{\mathrm{rec}}(l_d,\,j_d))$$

and for $l\in\mathbb{N}_0$ and $j\in\mathbb{Z}$ we set

$$\Theta_{\mathrm{rec}}(l,\,j):=\begin{cases}|j|, & \text{for } l=0,\\ |\frac{1}{2}+j| & \text{otherwise.}\end{cases}$$

Finally we define the *triangle* space $\Omega^{\mathcal{A}^{(N,S)}}_{\Lambda^{\mathrm{tri}}(L,J,R)}$ with help of

$$\Theta_{\mathrm{tri}}(\boldsymbol{l},\,\boldsymbol{j}):=(\Theta_{\mathrm{tri}}(l_1,\,j_1),\ldots,\Theta_{\mathrm{tri}}(l_d,\,j_d))$$

where for $l\in\mathbb{N}_0$ and $j\in\mathbb{Z}$ we set

$$\Theta_{\mathrm{tri}}(l,\,j):=\begin{cases}\frac{|j|}{1-\frac{l}{L_{\max}+1}} & \text{for } l=0,\\ \frac{|\frac{1}{2}+j|}{1-\frac{l}{L_{\max}+1}} & \text{for } 0<l\leq L_{\max},\\ \infty & \text{otherwise}\end{cases}$$

with $L_{\max}$ as the maximum level for the respective triangle.

Let us now discuss the results of our first, very preliminary numerical experiments with these new sparse grid methods for Schrödinger's equation. To this end, we restrict ourselves for complexity reasons to the case of one-dimensional particles only. The general three-dimensional case will be the subject of a forthcoming paper. We use in the following in (1) the potential

$$V=-\sum_{p=1}^{N}\sum_{q=1}^{N_{\mathrm{nuc}}}Z_q\,v(\boldsymbol{x}_p-\boldsymbol{R}_q)+\sum_{p=1}^{N}\sum_{q>p}^{N}v(\boldsymbol{x}_p-\boldsymbol{x}_q)\tag{35}$$

with

$$v(\boldsymbol{r})=\begin{cases}D-|\boldsymbol{r}|_2 & \text{for } |\boldsymbol{r}|_2\leq D,\\ 0 & \text{otherwise}\end{cases}$$

which is truncated at radius D and shifted by D. Note that $\lim_{|\boldsymbol{r}|_2\to\infty}v(\boldsymbol{r})=0$. Up to truncation and the shift with D, $|\boldsymbol{r}|_2$ is just the one-dimensional analogue to the

Coulomb potential. The Fourier transform reads

$$\hat{v}(\boldsymbol{k}) = \begin{cases} \frac{\sqrt{2}}{\sqrt{\pi}} \frac{1}{|\boldsymbol{k}|_2^2}(1 - \cos(D|\boldsymbol{k}|_2)) & \text{for } |\boldsymbol{k}|_2 \neq 0, \\ \frac{D^2}{\sqrt{2\pi}} & \text{otherwise.} \end{cases}$$

Note that $\hat{v}$ is continuous.

We study for varying numbers N of particles the behavior of the discrete energy E, i.e. the smallest eigenvalue of the associated system matrix A, as L and J increase. Here, we use the generalized antisymmetric sparse grids $\Omega^{\mathcal{A}^{(N,S)}}_{\Lambda^{\text{full}}(L,J,R)}$, $\Omega^{\mathcal{A}^{(N,S)}}_{\Lambda^{\Theta_{\text{rec}}}(L,J,R)}$ and $\Omega^{\mathcal{A}^{(N,S)}}_{\Lambda^{\Theta_{\text{tri}}}(L,J,R)}$ and focus on the two cases $S = 0$ or $S = \lfloor N/2 \rfloor$. We employ the Meyer wavelets with (9) where ν^∞, $\alpha = 2$, and the Shannon wavelet with ν^0 from (8). Tables 1 and 2 give the obtained results. Here, M denotes the number of degrees of freedom and $\#A$ denotes the number of the non-zero matrix entries. Furthermore, ΔE denotes the difference of the obtained values of E and ε denotes the quotient of the values of ΔE for two successive rows in the table. Thus, ε indicates the convergence rate of the discretization error.

Table 1. $d = 1$, $N = 1$, $c = 1$, $R = 1$, $\alpha_1 = 1$, $L_{\max} = L$, $D = 8$.

$\Omega^{\mathcal{A}^{(N,S)}}_{\Lambda^{\text{full}}(L,J,R)}$				ν^∞			ν^0		
J	L	M	$\#A$	E	ΔE	ε	E	ΔE	ε
2	1	5	25	−7.187310			−7.186261		
4	1	9	81	−7.189322	2.01e−03		−7.188615	2.35e−03	
8	1	17	289	−7.189334	1.14e−05	175.1	−7.188674	5.92e−05	39.7
16	1	33	1089	−7.189335	1.08e−06	10.6	−7.188683	9.25e−06	6.4
32	1	65	4225	−7.189335	4.60e−07	2.3	−7.188684	1.29e−06	7.1
64	1	129	16641	−7.189335	1.36e−09	336.4	−7.188685	1.73e−07	7.4
16	1	33	1089	−7.189335			−7.188683		
16	2	65	4225	−7.191345	2.00e−03		−7.190920	2.23e−03	
16	3	129	16641	−7.191376	3.19e−05	62.9	−7.190958	3.80e−05	58.7
16	4	257	66049				−7.190959	1.00e−06	37.6
16	5	513	263169				−7.190959	3.04e−08	33.1
$\Omega^{\mathcal{A}^{(N,S)}}_{\Lambda^{\Theta_{\text{rec}}}(L,J,R)}$				ν^∞			ν^0		
J	L	M	$\#A$	E	ΔE	ε	E	ΔE	ε
16	1	33	1089	−7.189335			−7.188683		
16	2	65	4225	−7.191345	2.00e−03		−7.190920	2.23e−03	
16	3	97	9409	−7.191376	3.19e−05	62.9	−7.190956	3.61e−05	61.8
16	4	129	16641	−7.191377	8.37e−07	38.0	−7.190957	9.52e−07	37.9
16	5	161	25921	−7.191377	2.51e−08	33.3	−7.190957	2.85e−08	33.3
16	6	193	37249	−7.191377	7.53e−10	33.4	−7.190957	8.84e−10	32.2
$\Omega^{\mathcal{A}^{(N,S)}}_{\Lambda^{\Theta_{\text{tri}}}(L,J,R)}$				ν^∞			ν^0		
J	L	M	$\#A$	E	ΔE	ε	E	ΔE	ε
16	1	33	1089	−7.189335			−7.189335		
16	2	55	3025	−7.191314	1.97e−03		−7.190747	1.41e−03	
16	3	73	5329	−7.191357	4.25e−05	46.5	−7.190825	7.80e−05	18.0
16	4	91	8281	−7.191366	9.28e−06	4.5	−7.190865	4.04e−05	1.9
16	5	107	11449	−7.191366	2.13e−07	43.4	−7.190866	5.42e−07	74.5
16	6	125	15625	−7.191371	5.07e−06	0.042	−7.190900	3.39e−05	0.016

In Table 1, with just one particle, i.e. $N = 1$, we see that the minimal eigenvalues for the Shannon wavelet are slightly, i.e. by $10^{-3} - 10^{-2}$, worse than the minimal eigenvalues for the Meyer wavelet with ν^∞. Furthermore, from the first part of the table where we fix $L = 1$ and vary J and alternatively fix $J = 16$ and vary L it gets clear that it necessary to increase both J *and* L to obtain convergence. While just an increase of J with fixed $L = 1$ does not improve the result at all (with D fixed), the increase of L for a fixed J at least gives a convergence to the solution on a bounded domain whose size is associated to the respective value of D and J. In the second part of the table we compare the behavior for $\Omega^{\mathcal{A}^{(N,S)}}_{\Lambda^{\text{full}}(L,J,R)}$ and $\Omega^{\mathcal{A}^{(N,S)}}_{\Lambda^{\Theta_{\text{rec}}}(L,J,R)}$ for the wavelets with ν^∞ and ν^0. While we see relatively stable monotone rates of around 33 and better in case of $\Omega^{\mathcal{A}^{(N,S)}}_{\Lambda^{\text{full}}(L,J,R)}$, the convergence behavior for $\Omega^{\mathcal{A}^{(N,S)}}_{\Lambda^{\Theta_{\text{rec}}}(L,J,R)}$ is more erratic. Nevertheless, when we compare the achieved results for the same amount of matrix entries $\#A$ we see not much difference. For example, with ν^∞, we get for $J = 16, L = 6$ with 125 degrees of freedom and 15625 matrix entries a value of -7.191371 for $\Omega^{\mathcal{A}^{(N,S)}}_{\Lambda^{\Theta_{\text{rec}}}(L,J,R)}$ whereas we get for $\Omega^{\mathcal{A}^{(N,S)}}_{\Lambda^{\text{full}}(L,J,R)}$ with $J = 16, L = 4$ with about the same degrees of freedom and matrix entries nearly the same value -7.191377.

Let us now consider the results for $N > 1$ given in Table 2. Here we restricted ourself to the sparse grid $\Omega^{\mathcal{A}^{(N,S)}}_{\Lambda^{\Theta_{\text{tri}}}(L,J,R)}$ due to complexity reasons. We see that the computed minimal eigenvalues in the case $S = \frac{N}{2}$ are higher than that in the case $S = 0$, as to be expected. Furthermore, our results suggest convergence for rising L. If we compare the cases $R = 1$ and $R = 2^{\frac{3}{2}}$ for $N = 2$, we see that both the number of degrees of freedom and the minimal eigenvalues are for $R = 1$ approximately the same as for $R = 2^{\frac{3}{2}}$ on the next coarser level. An analogous observation holds in the case $N = 4$.

Note furthermore that the sparse grid effect acts only on the fully antisymmetric subspaces of the total space. This is the reason for the quite large number of degrees of freedom for the case $N = 4$, $S = 2$.

Note finally that our present simple numerical quadrature procedure is relatively expensive. To achieve results for higher numbers of particles with sufficiently large L and J, the numerical integration scheme has to be improved. Moreover, to deal in the future with the case of three-dimensional particles using the classical potential (2) and the Meyer wavelets with ν^∞, an efficient and accurate numerical quadrature still has to be derived.[5]

[5]Such a numerical quadrature scheme must be able to cope with oscillatory functions and also must resolve the singularity in the Coulomb operator.

Table 2. $d = 1$, $c = 1$, $D = 8$, $\Omega^{\mathcal{A}^{(N,S)}}_{\Lambda^{\Theta_{\text{tri}}}(L,J,R)}$, ν^0.

$Z = 2$, $N = 2$, $S = 1$, $R = 1$, $\alpha_1 = \alpha_2 = \beta_{1,2} = \frac{1}{2}$						
J	L	M	$\#A$	E	ΔE	ε
8	4	1037	1029529	−28.818529		
8	5	1401	1788305	−28.819933	1.40e−03	
8	6	1623	2324081	−28.819954	2.07e−05	67.55
8	7	1943	3240369	−28.819963	8.81e−06	2.35
$Z = 2$, $N = 2$, $S = 1$, $R = 2^{\frac{3}{2}}$, $\alpha_1 = \alpha_2 = \beta_{1,2} = \frac{1}{2}$						
J	L	M	$\#A$	E	ΔE	ε
8	3	1067	1092649	−28.818529		
8	4	1425	1856129	−28.819933	1.40e−03	
8	5	1637	2369721	−28.819954	2.07e−05	67.55
8	6	1957	3829849	−28.819963	8.81e−06	2.35
$Z = 2$, $N = 2$, $S = 0$, $R = 1$, $\alpha_1 = \alpha_2 = \beta_{1,2} = \frac{1}{2}$						
J	L	M	$\#A$	E	ΔE	ε
8	4	383	138589	−27.134075		
8	5	501	234965	−27.134725	6.49e−04	
8	6	614	341696	−27.134725	3.98e−07	1630.99
8	7	731	470569	−27.134725	3.77e−07	1.05
$Z = 2$, $N = 2$, $S = 0$, $R = 2^{\frac{3}{2}}$, $\alpha_1 = \alpha_2 = \beta_{1,2} = \frac{1}{2}$						
J	L	M	$\#A$	E	ΔE	ε
8	3	475	215125	−27.134075		
8	4	622	353684	−27.134725	6.49e−04	
8	5	714	455420	−27.134725	3.98e−07	1631.10
8	6	852	624244	−27.134725	3.77e−07	1.05
$Z = 4$, $N = 4$, $S = 2$, $R = 1$, $\alpha_p = \beta_{p,q} = \frac{1}{4}$						
J	L	M	$\#A$	E	ΔE	ε
8	4	24514	17003256	−106.755154		
8	5	39104	32716440	−106.756364	1.20e−03	
$Z = 4$, $N = 4$, $S = 2$, $R = 8$, $\alpha_p = \beta_{p,q} = \frac{1}{4}$						
J	L	M	$\#A$	E	ΔE	ε
8	1	31592	22864800	−106.755154		
$Z = 4$, $N = 4$, $S = 0$, $R = 1$, $\alpha_p = \beta_{p,q} = \frac{1}{4}$						
J	L	M	$\#A$	E	ΔE	ε
8	4	1903	313963	−102.659381		
8	5	2842	647688	−102.659503	1.22e−04	
8	6	4039	1063101	−102.660489	9.86e−04	0.12
$Z = 4$, $N = 4$, $S = 0$, $R = 8$, $\alpha_p = \beta_{p,q} = \frac{1}{4}$						
J	L	M	$\#A$	E	ΔE	ε
8	1	3527	761851	−102.659381		
8	2	6029	1558219	−102.659503	1.22e−04	
8	3	8098	2343162	−102.660489	9.85e−04	0.12

8. Concluding remarks

In this article we proposed to use Meyer's wavelets in a sparse grid approach for a direct discretization of the electronic Schrödinger equation. The sparse grid constructions promises to break the curse of dimensionality to some extent and may allow a numerical treatment of the Schrödinger equation without resorting to any model approximation. We discussed the Meyer wavelet family and their properties and built on them an anisotropic multiresolution analysis for general particle spaces. Furthermore

we studied a semidiscretization with respect to the level and introduced generalized semidiscrete sparse grid spaces. We then restricted these spaces to the case of anti-symmetric functions with additional spin. Using regularity and decay properties of the eigenfunctions of the Schrödinger operator we discussed rescaled semidiscrete sparse grid spaces due to Yserentant. They allow to get rid of the terms that involve the $\mathcal{H}^{1,1}_{\text{mix}}$- and $\mathcal{H}^{1/2,1}_{\text{mix}}$-norm of the eigenfunction which may grow exponentially with the number of electrons present in the system. Thus a direct estimation of the approximation error can be achieved that only involves the $\mathcal{L}^2$-norm of the eigenfunction. We also showed that a Fourier series approximation of a splitting of the eigenfunctions living on a scaled hyperbolic cross in Fourier space essentially just results in Meyer wavelets. Therefore, we directly tried to discretize Schrödinger's equation in properly chosen wavelet subspaces.

We only presented preliminary numerical results with one-dimensional particles and a shifted and truncated potential. For the Meyer wavelets with ν^∞ and for the classical, not truncated Coulomb potential, substantially improved quadrature routines have to be developed in the future to achieved reasonable run times for the set up of the stiffness matrix. Furthermore, the interplay and the optimal choice of the coarsest scale, i.e. of c, the scaling parameter R, the domain truncation parameter J, the scale truncation parameter L and the parameters $L_{\max}$, α_p, $\beta_{p,q}$ is not clear at all and needs further investigation. Finally more experiments are necessary with other types of sparse grid subspaces beyond the ones derived from the Hylleraas-type function (34) to complete our search for an accurate and cost effective approximation scheme for higher numbers N of electrons. Probably not the best strategy for subspace selection was yet used and substantially improved schemes can be found in the future. This may be done along the lines of best M-term approximation which, from a theoretical point of view, would however involve a new, not yet existing Besov regularity theory for high-dimensional spaces in an anisotropic setting. Or, from a practical point of view, this would involve new adaptive sparse grid schemes using tensor product Meyer wavelets which need proper error estimators and refinement strategies for both the boundary truncation error and, balanced with it, the scale truncation error.

The sparse grid approach is based on a tensor product construction which allows to treat the nucleus–electron cusps properly which are aligned to the particle-coordinate axes of the system but which does not fit to the "diagonal" directions of the electron–electron cusps. Here, proper a-priori refinement or general adaptivity must be used which however involves for $d = 3$ at least the quite costly resolution of three-dimensional manifolds in six-dimensional space which limits the approach. To this end, new features have to brought into the approximation like for example wavelets which allow additionally for multivariate rotations in the spirit of curvelets [14]. Also an approach in the spirit of wave-ray multigrid methods [9] may be envisioned. Alternatively an embedding in still higher-dimensional formulations which allows to express the electron-electron pairs as new coordinate directions might be explored. This, however, is future work.

References

[1] Adams, R., *Sobolev spaces*. Academic Press, New York 1975.

[2] Agmon, S., *Lectures on exponential decay of solutions of second-order elliptic equations: Bounds on eigenfunctions of N-body Schrödinger operators*. Math. Notes 29, Princeton University Press, Princeton 1982.

[3] Atkins, P., and Friedman, R., *Molecular quantum mechanics*. Oxford University Press, Oxford 1997.

[4] Auscher, P., Weiss, G., and Wickerhauser, G., Local sine and cosine bases of Coifman and Meyer and the construction of smooth wavelets. In *Wavelets: A tutorial in theory and applications* (ed. by C. K. Chui), Academic Press, New York 1992, 237–256.

[5] Babenko, K., Approximation by trigonometric polynomials in a certain class of periodic functions of several variables. *Dokl. Akad. Nauk SSSR* **132** (1960), 672–675; English transl. *Soviet Math. Dokl.* **1** (1960), 672–675.

[6] Balay, S., Buschelman, K., Eijkhout, V., Gropp, W., Kaushik, D., Knepley, M., McInnes, L., Smith, and Zhang, H., PETSc users manual. Tech. Report ANL-95/11 - Revision 2.1.5, Argonne National Laboratory, 2004.

[7] Balian, R., Un principe d'incertitude fort en théorie du signal on mécanique quantique. *C. R. Acad. Sci. Paris Sér. II* **292** (1981), 1357–1361.

[8] Bellmann, R., *Adaptive control processes: A guided tour*. Princeton University Press, Princeton 1961.

[9] Brandt, A., and Livshits, I., Wave-ray multigrid method for standing wave equations. Electron. *Trans. Numer. Anal.* **6** (1997), 162–181.

[10] Le Bris, C., Computational chemistry from the perspective of numerical analysis. *Acta Numer.* **14** (2005), 363–444.

[11] Bungartz, H., and Griebel, M., A note on the complexity of solving Poisson's equation for spaces of bounded mixed derivatives. *J. Complexity* **15** (1999), 167–199.

[12] Bungartz, H., and Griebel, M., Sparse grids. *Acta Numer.* **13** (2004), 147–269.

[13] Cai, Z., Mandel, J., and McCormick, S., Multigrid methods for nearly singular linear equations and eigenvalue problems. *SIAM J. Numer. Anal.* **34** (1997), 178–200.

[14] Candés, E., and Donoho, D., Ridgelets: a key to higher-dimensional intermittency? *Phil. Trans. Roy. Soc. London Ser. A* **357** (1999), 2495–2509.

[15] Chan, T., and Sharapov, I., Subspace correction multi-level methods for elliptic eigenvalue problems. *Numer. Linear Algebra Appl.* **9** (1) (2002), 1–20.

[16] Chandrasekhar, S., and Herzberg, G., Energies of the ground states of He, Li^+, and O^{6+}. *Phys. Rev.* **98** (4) (1955), 1050–1054.

[17] Coifman, R., and Meyer, Y., Remarques sur l'analyse de Fourier à fenêtre. *C. R. Acad. Sci. Paris Sér. I Math.* **312** (1991), 259–261.

[18] Condon, E., The theory of complex spectra. *Phys. Rev.* **36** (7) (1930), 1121–1133.

[19] Daubechies, I., *Ten lectures on wavelets*. CBMS-NSF Regional Conf. Series in Appl. Math. 61, SIAM, Philadelphia 1992.

[20] Daubechies, I., Jaffard, S., and Journé, J., A simple Wilson orthonormal basis with exponential decay. *SIAM J. Math. Anal.* **24** (1990), 520–527.

[21] DeVore, R., Konyagin, S., and Temlyakov, V., Hyperbolic wavelet approximation. *Constr. Approx.* **14** (1998), 1–26.

[22] Feynman, R., There's plenty of room at the bottom: An invitation to enter a new world of physics. *Engineering and Science* **XXIII** (Feb. issue) (1960), http://www.zyvex.com/nanotech/feynman.html.

[23] Fliegl, H., Klopper, W., and Hättig, C., Coupled-cluster theory with simplified linear-r12 corrections: The CCSD(R12) model. *J. Chem. Phys.* **122** (8) (2005), 084107.

[24] Frank, K., Heinrich, S., and Pereverzev, S., Information complexity of multivariate Fredholm equations in Sobolev classes. *J. Complexity* **12** (1996), 17–34.

[25] Froese, R., and Herbst, I., Exponential bounds and absence of positive eigenvalues for N-body Schrödinger-operators. *Comm. Math. Phys.* **87** (3) (1982), 429–447.

[26] Garcke, J., and Griebel, M., On the computation of the eigenproblems of hydrogen and helium in strong magnetic and electric fields with the sparse grid combination technique. *J. Comput. Phys.* **165** (2) (2000), 694–716.

[27] Gerstner, T., and Griebel, M., Numerical integration using sparse grids. *Numer. Algorithms* **18** (1998), 209–232.

[28] Gerstner, T., and Griebel, M., Dimension–adaptive tensor–product quadrature. *Computing* **71** (1) (2003), 65–87.

[29] Griebel, M., Sparse grids and related approximation schemes for higher dimensional problems. In *Proceedings of the Conference on Foundations of Computational Mathematics* (FoCM05), Santander, Spain, 2005.

[30] Griebel, M., and Hamaekers, J., Sparse grids for the Schrödinger equation. *Math. Model. Numer. Anal.*, submitted.

[31] Griebel, M., and Knapek, S., Optimized tensor-product approximation spaces. *Constr. Approx.* **16** (4) (2000), 525–540.

[32] Griebel, M., Oswald, P., and Schiekofer, T., Sparse grids for boundary integral equations. *Numer. Math.* **83** (2) (1999), 279–312.

[33] Hackbusch, W., The efficient computation of certain determinants arising in the treatment of Schrödinger's equation. *Computing* **67** (2000), 35–56.

[34] Hernández, E., and Weiss, G., *A first course on wavelets*. Stud. Adv. Math., CRC Press, Boca Raton 1996.

[35] Hernandez, V., Roman, J., and Vidal, V., SLEPc: A scalable and flexible toolkit for the solution of eigenvalue problems. *ACM Trans. Math. Software* **31** (3) (2005), 351–362.

[36] Hochmuth, R., Wavelet bases in numerical analysis and restricted nonlinear approximation. Habilitationsschrift, Freie Universität Berlin, 1999.

[37] Hoffmann-Ostenhof, M., Hoffmann-Ostenhof, T., and Sørensen, T., Electron wavefunction and densities for atoms. *Ann. Henri Poincaré* **2** (2001), 77–100.

[38] Hunziker, W., and Sigal, I., The quantum N-body problem. *J. Math. Phys.* **41** (2000), 3448–3510.

[39] Jaffard, S., Meyer, Y., and Ryan, R., *Wavelets: Tools for science and technology*. SIAM, Philadelphia, PA, 2001.

[40] Kaiblinger, N., and Madych, W., Orthonormal sampling functions. *Appl. Comput. Harmon. Anal.*, to appear.

[41] Klopper, W., r12-dependent wavefunctions. In *The Encyclopedia of Computational Chemistry* (ed. by P. von Ragué Schleyer, N. L. Allinger, T. Clark, J. Gasteiger, P. A. Kollman, H. F. Schaefer, and P. R. Schreiner), John Wiley and Sons, Chichester 1998, 2351–2375.

[42] Knapek, S., Approximation und Kompression mit Tensorprodukt-Multiskalenräumen. Dissertation, Universität Bonn, 2000.

[43] Knapek, S., Hyperbolic cross approximation of integral operators with smooth kernel. Tech. Report 665, SFB 256, Universität Bonn, 2000.

[44] Knyazev, A., and Neymeyr, K., Efficient solution of symmetric eigenvalue problem using multigrid preconditioners in the locally optimal block conjugate gradient method. *Electron. Trans. Numer. Anal.* **15** (2003), 38–55.

[45] Lemarié, P., and Meyer, Y., Ondelettes et bases hilbertiennes. *Rev. Mat. Iberoamericana* **2** (1–2) (1986), 1–18.

[46] Levine, I., *Quantum chemistry*. 5th ed., Prentice-Hall, 2000.

[47] Livne, O., and Brandt, A., $O(N \log N)$ multilevel calculation of N eigenfunctions. In *Multiscale Computational Methods in Chemistry and Physics* (ed. by A. Brandt, J. Bernholc, and K. Binder), NATO Science Series III: Computer and Systems Sciences 177, IOS Press, 2001, 112–136.

[48] Low, F., Complete sets of wave packets. In *A Passion for Physics—Essays in Honor of Geoffrey Chew*, World Scientific, Singapore 1985, 17–22.

[49] Malvar, H., Lapped transform for efficient transform/subband coding. *IEEE Trans. Acoust. Speech Signal Process.* **38** (1990), 969–978.

[50] Mazziotti, D., Variational two-electron reduced density matrix theory for many-electron atoms and molecules: Implementation of the spin- and symmetry-adapted T-2 condition through first-order semidefinite programming. *Phys. Rev. A* **72** (3) (2005), 032510.

[51] Messiah, A., *Quantum mechanics*. Vol. 1, 2, North-Holland, Amsterdam 1961/62.

[52] Meyer, Y., *Wavelets and operators*. Cambridge Stud. Adv. Math. 37, Cambridge University Press, Cambridge 1992.

[53] Meyer, Y., *Wavelets, vibrations and scalings*. CRM Monograph Ser.9, Amer. Math. Soc., Providence, RI, 1998.

[54] Pan, G., *Wavelets in electromagnetics and device modeling*. Wiley–IEEE Press, 2003.

[55] Parr, R., and Yang, W., *Density functional theory of atoms and molecules*. Oxford University Press, New York 1989.

[56] Persson, A., Bounds for the discrete part of the spectrum of a semi-bounded Schrödinger operator. *Math. Scand.* **8**, (1960), 143–153.

[57] Rodriguez, K., and Gasaneo, G., Accurate Hylleraas-like functions for the He atom with correct cusp conditions. *J. Phys. B: At. Mol. Opt. Phys.* **38** (2005), L259–L267.

[58] Schmeisser, H., and Triebel, H., *Fourier analysis and functions spaces*. John Wiley, Chichester 1987.

[59] Simon, B., Schrödinger operators in the twentieth century. *J. Math. Phys.* **41** (2000), 3523–3555.

[60] Slater, J., The theory of complex spectra. *Phys. Rev.* **34** (10) (1929), 1293–1322.

[61] Smolyak, S., Quadrature and interpolation formulas for tensor products of certain classes of functions. *Dokl. Akad. Nauk SSSR* **148** (1963), 1042–1045; English. transl. *Soviet Math. Dokl.* **4** (1963), 240–243.

[62] Walnut, D., *An introduction to wavelet analysis*. Appl. Numer. Harmon. Anal., Birkhäuser, Boston 2002.

[63] Walter, G., and Zhang, J., Orthonormal wavelets with simple closed-form expressions. *IEEE Trans. Signal Process.* **46** (8) (1998), 2248–2251.

[64] Wilson, K., Renormalization group and critical phenomena. II. Phase-space cell analysis of critical behavior. *Phys. Rev. B* **4** (1971), 3184–3205.

[65] Yamada, M., and Ohkitani, K., An identification of energy cascade in turbulence by orthonormal wavelet analysis. *Prog. Theor. Phys.* **836** (4) (1991), 799–815.

[66] Yserentant, H., On the electronic Schrödinger equation. Report 191, SFB 382, Universität Tübingen, 2003.

[67] Yserentant, H., On the regularity of the electronic Schrödinger equation in Hilbert spaces of mixed derivatives. *Numer. Math.* **98** (2004), 731–759.

[68] Yserentant, H., Sparse grid spaces for the numerical solution of the electronic Schrödinger equation. *Numer. Math.* **101** (2005), 381–389.

[69] Yserentant, H., The hyperbolic cross space approximation of electronic wavefunctions. *Numer. Math.* submitted.

[70] Yserentant, H., The hyperbolic cross space approximation of electronic wavefunctions. Talk at IHP-EU Network Workshop/Winter School Breaking Complexity: Nonlinear/Adaptive Approximation in High Dimensions, Physikzentrum Bad Honnef, Germany, 15th December 2005.

Institut für Numerische Simulation, Universität Bonn, Wegelerstr. 6, 53115 Bonn, Germany
E-mail: griebel@ins.uni-bonn.de

Institut für Numerische Simulation, Universität Bonn, Wegelerstr. 6, 53115 Bonn, Germany
E-mail: hamaeker@ins.uni-bonn.de